NASA TECHNICAL NOTE

NASA TN D-5921

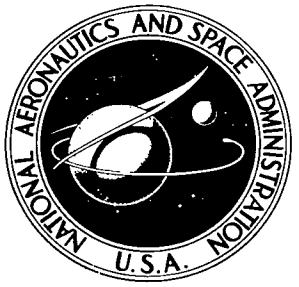

NASA TN D-5921

c.1

LOAN COPY: RETURN TO
AFWL (WLOL)
KIRTLAND AFB, N MEX

TECH LIBRARY KAFB, NM
0132790

EFFECTS OF A POINTED NOSE ON SPIN CHARACTERISTICS OF A FIGHTER AIRPLANE MODEL INCLUDING CORRELATION WITH THEORETICAL CALCULATIONS

by Joseph R. Chambers, Ernie L. Anglin, and James S. Bowman, Jr.

Langley Research Center
Hampton, Va. 23365

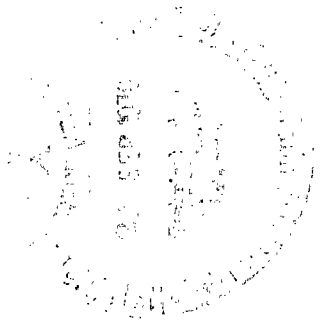

NATIONAL AERONAUTICS AND SPACE ADMINISTRATION • WASHINGTON, D. C. • SEPTEMBER 1970

TECH LIBRARY KAFB, NM
0132790

1. Report No.	2. Government Accession No.	3. Recipie
NASA TN D-5921		

4. Title and Subtitle
EFFECTS OF A POINTED NOSE ON SPIN CHARACTERISTICS OF A FIGHTER AIRPLANE MODEL INCLUDING CORRELATION WITH THEORETICAL CALCULATIONS

5. Report Date
September 1970

6. Performing Organization Code

7. Author(s)
Joseph R. Chambers, Ernie L. Anglin, and James S. Bowman, Jr.

8. Performing Organization Report No.
L-7325

10. Work Unit No.
126-62-11-01

9. Performing Organization Name and Address
NASA Langley Research Center
Hampton, Va. 23365

11. Contract or Grant No.

13. Type of Report and Period Covered
Technical Note

12. Sponsoring Agency Name and Address
National Aeronautics and Space Administration
Washington, D.C. 20546

14. Sponsoring Agency Code

15. Supplementary Notes

16. Abstract

An investigation was conducted to correlate the results of theoretical spin calculations with the results of free-flight model tests for a contemporary fighter configuration. The study was designed to substantiate the theoretical methods before these methods are applied to studies of the spin and recovery characteristics of the airplane. In order to explain some of the results obtained, however, a series of wind-tunnel tests which produced significant information on the effects of a long pointed fuselage nose on spin characteristics was conducted. Various techniques employed in the study included static and forced-oscillation wind-tunnel tests, theoretical calculations, flow-visualization tests, autorotation tests, and free-spinning tests of dynamically scaled models.

17. Key Words (Suggested by Author(s))
Spinning
Yawing moments
High angles of attack
Analytical techniques

18. Distribution Statement
Unclassified – Unlimited

19. Security Classif. (of this report)	20. Security Classif. (of this page)	21. No. of Pages	22. Price*
Unclassified	Unclassified	57	$3.00

*For sale by the Clearinghouse for Federal Scientific and Technical Information
Springfield, Virginia 22151

EFFECTS OF A POINTED NOSE ON SPIN CHARACTERISTICS OF A FIGHTER AIRPLANE MODEL INCLUDING CORRELATION WITH THEORETICAL CALCULATIONS

By Joseph R. Chambers, Ernie L. Anglin,
and James S. Bowman, Jr.
Langley Research Center

SUMMARY

An investigation was conducted to correlate the results of theoretical spin calculations with the results of free-flight model tests for a contemporary fighter configuration. The study was designed to substantiate the theoretical methods before these methods were applied to studies of the spin and recovery characteristics of the airplane. In order to explain some of the results obtained, however, a series of wind-tunnel tests which produced significant information on the effects of a long pointed fuselage nose on spin characteristics was conducted. Various techniques employed in the study included static and forced-oscillation wind-tunnel tests, theoretical calculations, flow-visualization tests, autorotation tests, and free-spinning tests of dynamically scaled models.

The results of the study indicated that extremely poor correlation existed between the results of theoretical calculations and the results obtained during free-flight tests because of large, random asymmetric yawing moments at high angles of attack. The large asymmetric moments were produced by asymmetric vortex sheets that were shed off the long pointed nose of the configuration at high angles of attack. The sense of the asymmetric moments could be controlled by nose strakes. Aerodynamic characteristics of the nose also produced large propelling values of aerodynamic damping in yaw at high angles of attack which promoted autorotational tendencies. Results of limited spin-tunnel tests indicated that strakes placed on the nose had little effect on the characteristics of a flat spin exhibited by the configuration when extended after the spin was developed, but extending the strakes before the flat spin was fully developed produced satisfactory recoveries when conventional spin-recovery control techniques were used. The results also indicated that in order to be most effective as spin-recovery devices for the present configuration, nose strakes should be deployed immediately after the stall and loss of control.

INTRODUCTION

The National Aeronautics and Space Administration is currently conducting a series of investigations to evaluate the spin and recovery characteristics of a contemporary fighter airplane equipped with a variable-sweep wing. These studies consist of: (1) spin-tunnel tests to determine the characteristics of developed spins and to evaluate techniques for recovery from fully developed spins; (2) analytical studies of the spin, including calculations of spin entry following departure from controlled flight; and (3) outdoor radio-controlled drop-model tests to provide flight data for correlation with the theoretical calculations.

The present part of the study was initially undertaken as a correlation of calculated spin characteristics with the results of the drop-model tests to substantiate the theoretical methods before they were applied to a broad analysis of the spin characteristics of the airplane. In order to explain some of the results obtained, however, a special series of wind-tunnel tests was conducted which has produced a body of information on the effects of the long pointed fuselage nose on spinning. These effects are of considerable importance in themselves. The present paper reports on both the spin-theory correlation and the studies of the effects of the fuselage nose on spin characteristics. The results of the study are meant to: (1) illustrate some of the factors that may limit usefulness of analytical treatments of the stall-spin problem for configurations with long pointed noses, (2) document the effects of geometric modifications designed to provide more acceptable spin characteristics for the particular airplane, and (3) provide a better understanding of aerodynamic characteristics exhibited by many contemporary fighter airplanes during spins.

SYMBOLS

All quantities are presented with respect to a body system of axes. Aerodynamic coefficients are based on the dimensional characteristics of the wing for a sweep angle of 16°. Data are referred to a center-of-gravity position of 45 percent wing mean aerodynamic chord (sweep angle, 16°). Dimensional values are given in U.S. Customary Units and in the International System of Units.

b wing span, ft (m)

$\bar{c}$ wing mean aerodynamic chord, ft (m)

C_m pitching-moment coefficient, $\frac{M_Y}{q_\infty S\bar{c}}$

$C_{m,i}$ inertial pitching-moment coefficient, $4\left(\frac{I_Z - I_X}{mb^2}\right)\left(\frac{\Omega b}{2V}\right)^2\left(\frac{b}{\bar{c}}\right)\mu_b \sin 2\alpha$

C_N normal-force coefficient, $\frac{F_N}{q_\infty S}$

C_n yawing-moment coefficient, $\frac{M_Z}{q_\infty Sb}$

C_Y side-force coefficient, $\frac{F_Y}{q_\infty S}$

F_N normal force, lb (N)

F_Y side force, lb (N)

I_X, I_Y, I_Z moments of inertia about X, Y, and Z body axes, slug-ft^2 (kg-m^2)

$\frac{I_Z - I_X}{mb^2}$ inertial pitching-moment parameter

m airplane mass, slugs (kg)

M_Y pitching moment about Y body axis, ft-lb (m-N)

M_Z yawing moment about Z body axis, ft-lb (m-N)

p,q,r angular velocities about X, Y, and Z body axis, rad/sec

q_∞ dynamic pressure, $\frac{1}{2}\rho V^2$, lb/ft^2 (N/m^2)

R Reynolds number based on mean aerodynamic chord

S wing area, ft^2 (m^2)

t time, sec

V resultant linear velocity, ft/sec (m/sec)

W	weight, lb (N)
x	distance along X-axis, ft (m)
α	angle of attack, deg
β	angle of sideslip, deg
Λ	wing leading-edge sweep angle, deg
μ_b	airplane relative density, $\frac{m}{\rho S b}$
ρ	air density, slug/ft^3 (kg/m^3)
Ω	resultant angular velocity, rad/sec
$\frac{\Omega b}{2V}$	nondimensional spin-rate coefficient
ϕ	angle between Y body axis and horizon measured in a vertical plane, positive for right wing down, deg
δ_a	aileron deflection, positive when trailing edge of right aileron is deflected downward, deg
δ_e	elevator deflection, positive when trailing edge is down, deg
δ_r	rudder deflection, positive when trailing edge is left, deg

Stability derivatives:

$$C_{m_q} = \frac{\partial C_m}{\partial \frac{q\bar{c}}{2V}} \qquad C_{m_{\dot{\alpha}}} = \frac{\partial C_m}{\partial \frac{\dot{\alpha}\bar{c}}{2V}} \qquad C_{N_q} = \frac{\partial C_N}{\partial \frac{q\bar{c}}{2V}} \qquad C_{N_{\dot{\alpha}}} = \frac{\partial C_N}{\partial \frac{\dot{\alpha}\bar{c}}{2V}}$$

$$C_{n_\beta} = \frac{\partial C_n}{\partial \beta} \qquad C_{Y_\beta} = \frac{\partial C_Y}{\partial \beta}$$

$$C_{n_r} = \frac{\partial C_n}{\partial \frac{rb}{2V}} \qquad C_{Y_r} = \frac{\partial C_Y}{\partial \frac{rb}{2V}}$$

$$C_{n_{\dot{\beta}}} = \frac{\partial C_n}{\partial \frac{\dot{\beta} b}{2V}} \qquad C_{Y_{\dot{\beta}}} = \frac{\partial C_Y}{\partial \frac{\dot{\beta} b}{2V}}$$

A dot over a symbol denotes differentiation with respect to time; for example, $\dot{\beta} = \frac{d\beta}{dt}$.

DESCRIPTION OF AIRPLANE

The airplane studied in the investigation was the two-place variable-sweep fighter shown in the three-view sketch of figure 1. Geometric characteristics of the airplane are listed in table I. A wing sweep angle of 50° was used for all the free-flight tests of the present investigation. The longitudinal control system of the airplane consists of an all-movable horizontal tail; the lateral control system consists of spoilers (operative through a wing-sweep range of 16° to 47°) and differential deflection of the horizontal-tail surfaces; and the directional control system consists of a conventional rudder. For simplicity, these controls are referred to herein as elevator, aileron, and rudder. The maximum control surface deflections are as follows:

Rudder deflection, deg	±7.5
Horizontal tail:	
Trailing edge up, deg	25
Trailing edge down, deg	10
Horizontal tail as roll control, deg	±8

Because most of the present study was conducted only for $\Lambda = 50^\circ$, the spoilers were inactive and the horizontal tail was the sole source of roll control.

Spin-Recovery Technique

Mass loading conditions for the present configuration are typical of those associated with contemporary fighter airplane designs inasmuch as the values of I_Z and I_Y are several times greater than those of I_X. As pointed out in reference 1, the most effective way to obtain antispin yawing moments for spin recovery of configurations having relatively low values of I_X may be to roll the airplane about the X body axis in such a direction as to produce an inertial antispin yawing moment.

The mechanism by which the antispin inertial moment is produced can be visualized with the aid of the sketches presented in figure 2. The lower sketch shows a side view of an airplane in a spin to the right with the wings level. The angular velocity Ω of the spin can be resolved into angular velocity components p and r about the X and Z body axes, respectively. The upper sketch shows the projected plan view of the airplane. The fuselage-heavy loading typical of contemporary fighter airplanes is represented by weights distributed along the X body axis. If the wings are maintained level, the angular velocity p will be the sole component of Ω in the XY plane of the vehicle during the steady spin. However, if the airplane is banked to the right by the use of ailerons, a component of Ω will be introduced into the XY plane as a positive rate of pitch q ($q \approx \Omega \sin \phi$). As depicted in the upper sketch, the angular velocities p and q combine vectorially to produce a component of rotation within the XY plane whose magnitude is given by $\sqrt{p^2 + q^2}$ and whose direction is indicated by the arrow. The heavy fuselage, acting similar to a dumbbell, tends to aline itself perpendicular to this component of rotation and, in so doing, creates a large angular deceleration which tends to retard the spin rate.

As a result of these considerations (which have been verified experimentally for a large number of airplane configurations), the proper spin-recovery control technique for the present configuration is simultaneous movement of the ailerons to full with the spin (stick right for a right spin), full-aft stick, and rudder full against the direction of rotation. The fact that this is the most effective recovery technique for the subject airplane has been verified both by the results of unpublished spin-tunnel tests and radio-controlled drop tests of models of the particular airplane.

Static and Forced-Oscillation Tests

Static and forced-oscillation tests were conducted with the 1/9-scale model used for the outdoor drop-model spin tests to obtain aerodynamic characteristics of the model over the range of angle of attack and angle of sideslip involved in the spin. The tests were conducted in the 30- by 60-foot (9.1- by 18.3-m) test section of the Langley full-scale tunnel at a Reynolds number of 0.7×10^6 based on the mean aerodynamic chord of the wing. This value of Reynolds number was approximately equal to that obtained for the developed spins during the drop-model flight tests. Measurements were made of the six force and moment components over an angle-of-attack range of -20° to 100° for a range of sideslip angle of $\pm 40^\circ$ and for the complete range of control deflections. The forced-oscillation tests consisted of tests with oscillations in pitch, roll, and yaw over a similar angle-of-attack range. The tests were conducted by using the apparatus and the technique described in reference 2. These tests were made for oscillation amplitudes of $\pm 5^\circ$ and $\pm 10^\circ$ for frequencies of 1.0 and 0.7 cycle per second.

Results obtained during static wind-tunnel tests of a number of other models of the configuration have been included in the analysis. In addition to the 1/9-scale free-flight model, a 1/10-scale model was tested in the Langley full-scale tunnel, and 1/15-scale and 1/24-scale models were tested in the Ames 12-foot pressure tunnel.

Additional tests were conducted to evaluate the effects of several modifications to the nose of the configuration. Some of these tests were directed at an evaluation of the effects of various nose strakes. Two of the more pertinent nose strake configurations are shown in figure 3. One strake arrangement, shown in figure 3(a), consisted of a single strake on one side of the nose only, the strake beginning at the apex of the nose and extending along the maximum diameter line of the nose. The second strake arrangement, shown in figure 3(b), was a double-strake configuration with strakes on each side of the nose located on the upper fuselage forebody at an angle of 40° relative to the maximum diameter line of the nose. These strake tests were conducted with the 1/9-scale and 1/10-scale models at the Langley Research Center. Tests were also conducted to determine the effects of nose tip shape on the aerodynamic characteristics. For these tests, the normal nose tip was replaced by the nose tips shown in figure 4. The relative size of the nose tips is indicated by the upper sketch of the airplane. Four nose tips were tested: the basic nose with a flat spot on the right side, the basic nose with a flat spot on the left side, a sharply pointed nose tip, and a rounded tip. These nose-tip tests were conducted with a 1/15-scale model in the Ames 12-foot pressure tunnel at several values of Reynolds number.

Autorotation Tests

Single-degree-of-freedom and two-degree-of-freedom autorotation tests were conducted by using the test setup shown in figure 5. In these tests a 1/10-scale model was mounted in a pivoted yoke which allowed freedom in pitch, and which was, in turn, mounted to a freely rotating sting. With this test setup, freedom about the spin axis and pitch axis could be obtained both individually and simultaneously. Autorotative tendencies of the basic airplane configuration with the sting in the plane of symmetry and the spin axis alined with the wind (and resulting in a sideslip angle of 0°) were investigated as well as autorotative characteristics with strakes added to the fuselage forebody. No measurements of aerodynamic forces or moments were made during the autorotation tests. These tests were conducted over an angle-of-attack range of 40° to 90°, and were made only for the 50° sweep configuration.

Flow-Visualization Tests

Flow-visualization tests were made in an effort to define more fully the aerodynamic phenomena at high angles of attack. These tests consisted of smoke studies with the model held at fixed attitudes.

Spin Tunnel and Outdoor Spin Tests

A limited number of tests with a 1/40-scale model were conducted in the Langley spin tunnel to determine the effects of the fuselage forebody on the spin characteristics of the configuration for $\Lambda = 50^{\circ}$. A number of nose-strake configurations, shown in figure 6, were evaluated with regard to effects on the developed spin and recovery characteristics. All strake configurations consisted of a single strake on the left side of the nose, and all spins were to the left. In these tests, the strakes were extended before the model was launched into the spin with the exception of strake 6, which was designed to be retractable to permit studies of strake deployment during developed spins. For the spin-tunnel tests, the dynamically scaled model was launched with prerotation, at an angle of attack of about 90°, into the vertically rising airstream. Additional details regarding the test technique used in the Langley spin tunnel are presented in reference 1.

In addition to the spin-tunnel tests, a series of outdoor flights was made with the 1/9-scale radio-controlled model to determine the spin entry, developed spin, and recovery characteristics of the basic configuration for correlation with calculated spin characteristics and also to determine the effects of the double-strake arrangement of figure 3 on the spin entry. The unpowered model was dropped from a helicopter with neutral controls. After the model was launched from the helicopter, the controls generally were moved to full pro-spin deflections (an extended rudder deflection of $\pm 25^{\circ}$ was used for the drop tests) in a deliberate attempt to put the model into a spin. Additional information on the radio-controlled technique is presented in reference 3.

METHOD OF APPROACH

As pointed out previously, the investigation consisted of: (1) a correlation of calculated spin characteristics with flight tests for a drop model, and (2) special wind-tunnel tests to investigate the cause of some of the results obtained. The methods used in this investigation are detailed in the following sections.

Theoretical Analysis and Verification

Spin entries and recoveries from spinning motions were calculated by a high-speed digital computer program which used numerical integration methods to solve nonlinear equations of motion representing six degrees of freedom along and about a body system of axes.

Aerodynamic data for the calculations were based on the results of static and forced oscillation tests of a 1/9-scale model of the airplane. Some of the more pertinent data obtained are presented in this report. The model used in the wind-tunnel tests had previously been equipped with radio-controlled instrumentation and was flown into spins

after it was released from a helicopter during a series of outdoor free-flight tests. The aerodynamic characteristics were measured for this model at approximately the same value of Reynolds number as that for the free-flight tests. The static aerodynamic forces and moments were incorporated into the computer program as nonlinear functions of angle of attack and angle of sideslip, whereas the dynamic aerodynamic characteristics were represented by conventional dynamic stability derivatives which were functions of angle of attack.

The calculations were performed by duplicating within the computer program the initial conditions and control input sequencing from flight records obtained during the free-flight tests. By using this procedure, it was possible to compare the spin characteristics exhibited by the model with analytical predictions of spin characteristics based on aerodynamic inputs measured with the same model at the same value of Reynolds number. The results of this correlation should therefore serve to determine the adequacy of theoretical spin studies for the present configuration.

RESULTS AND DISCUSSION

In brief, the results of the investigation showed very poor correlation between theoretical calculations of the spin entry and developed spin motions of the model and the actual motions of the model measured during the radio-controlled drop-model tests. The results of the various types of wind-tunnel tests indicated that a major reason for this lack of correlation was that the long pointed nose of the model caused large nonrepeatable yawing moments at high angles of attack. Because of the randomness of these yawing moments, a wide variety of different types of airplane motion might develop from any given set of initial conditions and control inputs. In addition, the results showed that the yawing moments produced by rate of yaw at high angles of attack were nonlinear with respect to the rate of rotation. These results are detailed in subsequent sections of the paper.

Correlation of Theoretical Results With Flight Tests

Throughout the analytical study, poor correlation existed between the calculated motions and the flight data obtained during the outdoor free-flight tests. For example, shown in figure 7 are comparisons of angle of attack, angle of sideslip, and rate of yaw as calculated by the computer program (solid lines) and as obtained from flight recorder traces (dashed lines) for three representative flights. Each flight involved pro-spin control inputs for a right spin (elevator full trailing edge up, ailerons against the spin, and rudder with the spin). The data show extremely poor correlation inasmuch as the magnitudes and variations of angle of attack, angle of sideslip, and yaw rate are markedly

different during the spin. In fact, the agreement was so poor that in some cases, such as that of figure 7(a), the theoretical results predicted a fast-flat spin whereas the free-flight model exhibited a steeper oscillatory spin of completely different character.

In view of the apparent inability of the analytical technique to predict adequately the spin characteristics of the model, additional wind-tunnel tests were undertaken to gain some insight into possible shortcomings of the theoretical representation of the aerodynamic forces and moments acting on the configuration during a spin. This paper describes the results of wind-tunnel tests and other pertinent data gathered during the investigation which produced several important results that appear to have been the cause of the poor correlation between theory and flight results.

Static and Forced Oscillation Tests

Asymmetric yawing moments.- The most significant result of the static force tests with regard to the lack of correlation between calculated and measured spin motions was an indication that large yawing moments existed for the present configuration at high angles of attack, and that these yawing moments appeared to be random and nonrepeatable. The large excursions of yawing moment are illustrated in figures 8 and 9. Figure 8 shows the variation of static yawing-moment coefficient C_n with angle of attack at zero sideslip and neutral controls as measured during tests of four separate models of the present configuration. As can be seen, the value of C_n remained near zero at low angles of attack, as might be expected. For angles of attack greater than about 30°, however, large excursions of C_n occurred. The magnitudes of these moments are best appreciated by comparison with the value indicated by the dashed line which indicates the magnitude of C_n produced by a full rudder deflection of 7.5° in the normal low angle-of-attack flight range. The out-of-trim moments near $\alpha = 60^\circ$ are several times as large as the moments produced by full-rudder deflection at low angles of attack, and would be much larger than moments obtained by rudder deflection at $\alpha = 60^\circ$ because of the marked reduction in rudder effectiveness at high angles of attack due to shielding by the fuselage and wing.

An equally important phenomenon exhibited by the configuration was the fact that these large asymmetric yawing moments appeared to be random and nonrepeatable, even for the same model under identical test conditions. A sample of this randomness is presented in figure 9, which presents the variation of C_n with angle of attack for $\beta = 0^\circ$ for repeat tests of a 1/10-scale model of the configuration at a Reynolds number of 0.3×10^6. The data indicate that for angles of attack above about 40°, separate tests under the same test conditions produced markedly different values of C_n with large excursions in both the sense and magnitude of the asymmetric moment. Examination of

the complete set of data for each of the four models for which data are presented in figure 8 indicated that similar random yawing moments occurred for all models at high angles of attack and that this scatter existed over a range of angle of sideslip of about $\pm 20^{\circ}$.

The effect of these large excursions of C_n on spin characteristics was evaluated by means of a series of theoretical calculations in which the asymmetry of C_n was assumed to have the maximum values indicated in figure 8 in either a nose-right or a nose-left sense. In these calculations, the airplane was initially in trimmed level flight followed by full pro-spin control deflections for a right spin (similar to the deflections shown in fig. 7). When the asymmetric values of C_n were assumed to have the maximum positive (nose right) values indicated in figure 8, the results of the calculations indicated that a flat-fast spin to the right was obtained. (The asymmetric values used in the calculations and shown in fig. 7 were also nose right.) When the sense of the asymmetry was reversed (that is, in a nose-left sense), the calculations indicated that the airplane would not spin to the right (even with full right pro-spin controls) but would instead perform large-amplitude poststall gyrations with no continuous rotation. These results show that, depending on the particular asymmetry present, a fast-flat spin or a no-spin condition (and, presumably any type of spin in between) could be obtained from identical initial conditions and control inputs. The large scatter of static yawing moment shown in figures 8 and 9 therefore creates a number of calculated flight motions from identical control inputs and this fact results in a severe limitation of the usefulness of analytical methods for spin studies of this particular configuration. This characteristic is believed to be a primary cause of the poor correlation previously shown between the theoretical spin calculations and the free-flight results.

Large out-of-trim yawing moments at high angles of attack similar to those measured in the present study have also been noted in past investigations of pointed bodies of revolution (refs. 4 to 8), highly swept delta wing-body combinations (ref. 9), and an airplane configuration having a long pointed nose (ref. 10). In all cases, the aerodynamic phenomenon producing the large yawing moments was attributed to asymmetrical shedding of vortex sheets off the long sharply pointed nose. The flow pattern of such vortices on the fuselage forebody with this type of flow separation is illustrated by the sketch in figure 10. Separation of flow from the fuselage forebody at low angles of attack is characterized by two shed vortex sheets. At angles of attack less than 20° for the present configuration, these vortex sheets remain nearly symmetrical above the nose, as depicted by the upper sketch, and are probably not very strong. Because of the symmetry of the vortex sheets, they do not induce asymmetric forces on the forebody for this condition. For angles of attack greater than 20°, however, the vortex sheet pattern becomes stronger and asymmetrical, as shown by the lower sketch; one vortex core moves above and away from the forebody whereas the other vortex core moves closer to the nose. The flow

pattern on the present configuration at $\alpha = 60^{\circ}$ is shown by the results of the flow-visualization tests presented in figure 11. The photograph in figure 11(a) is a three-quarter view looking forward. Smoke injected into the flow defines an asymmetric vortex pattern; one vortex core was observed to be high above and to the left of the nose and another vortex core, immediately above and to the right of the nose. The side view shown in figure 11(b) shows the relative vertical displacement of the two vortex cores. The asymmetric vortex pattern creates a large negative pressure area on one side of the nose and thereby creates a side force on the nose which, in turn, produces a large yawing moment because of the relatively long distance between the nose and the center of gravity of the airplane.

Experience has shown that a number of factors, such as the fineness ratio of the pointed nose, the cross-sectional shape of the nose, the distance between the nose and the center of gravity of the airplane, and the dimensional symmetry of the nose, can affect the asymmetric yawing moments at high angles of attack. The relative importance of the length and fineness ratio of the pointed nose is indicated by figure 12. Figure 12 shows the variation of C_n with angle of attack measured during recent tests at the Langley Research Center for the present configuration, a twin-jet swept-wing fighter with a relatively short low-fineness-ratio nose, and a fighter configuration having an unswept wing and a relatively long high-fineness-ratio nose. These data indicate that the unswept fighter configuration with a long pointed nose also exhibited large out-of-trim moments. However, the swept-wing fighter configuration with the shorter nose did not exhibit appreciable out-of-trim moments over the entire range of angle of attack.

The random out-of-trim moments result from the fact that some slight geometric or aerodynamic asymmetry establishes the sense of the asymmetric moment. For sharp, high-fineness-ratio noses, even very minor asymmetries near the apex of the nose can be very important. For example, experience gathered over a period of years from tests of many models in the Langley spin tunnel has shown that almost all airplane configurations having long sharp pointed noses (including the present configuration) may spin readily in one direction and not in the other until some slight deformation to the nose tip occurs during the tests after which the ease of achieving a spin in a given direction can reverse; subsequent deformation of the nose may cause this reversal to occur at various times during the course of a test program. The effect of slight asymmetry near the tip of the nose is illustrated by the data presented in figure 13 which presents the variation of C_n with α for the basic nose tip with a flat spot on the right side of the nose (see fig. 4) and for the basic nose with a flat spot on the left side of the nose. With the flat spot on the right side of the nose, the model exhibited large out-of-trim yawing moments to the left. With the nose tip flattened on the left side, however, the asymmetry was reversed, apparently because of a reversal in the pattern of the asymmetric vortex sheets shed by the nose. Several repeat tests with the flat spots on the nose produced consistent

results; that is, the sense and magnitudes of the yawing moments remained constant. Two points should be made regarding these results. First, the asymmetric moments are extremely sensitive to nose-tip imperfections, and second, geometric asymmetries tend to stabilize the sense of the moment at zero sideslip.

Additional tests were conducted to determine whether the asymmetric yawing moments would be minimized by altering the basic shape of the nose tip. Data measured with the basic, the sharply pointed, and the rounded nose tips (see fig. 4) at three values of Reynolds number are presented in figure 14. These data show that progressive rounding of a small section of the nose from a sharp conical tip to a rounded tip had little effect on the general tendency of the configuration to produce out-of-trim moments. This result was also noted in reference 10 wherein the sharp nose of another airplane configuration was also blunted. It appears, therefore, that the overall conical shape of the fuselage nose and the distance between the nose tip and the center of gravity of the airplane are more important than the apex angle of the extreme tip of the nose in producing large out-of-trim moments for this particular configuration. The data show that the asymmetric moment for the rounded nose reversed in sense as Reynolds number was increased; it should be kept in mind that this reversal is probably caused by nonrepeatability rather than variations in Reynolds number. The data of figure 14 show that the effect of Reynolds number was to reduce the magnitude of the out-of-trim moments and to cause them to peak at lower angles of attack as the Reynolds number was increased. The magnitudes of the asymmetric yawing moments at the highest Reynolds number tested, however, are still very large and could easily influence the spin characteristics of the full-scale airplane.

The previous discussion has emphasized that the present configuration at high angles of attack will experience large, random yawing moments which can have a large effect on the tendency of the configuration to spin. It appears that the usefulness of analytical studies of the spin for the present configuration is extremely limited; in particular, it does not appear to be possible to obtain even a qualitative check with results of spin tests, even though the aerodynamic data used for input are measured on the same model at the same Reynolds number as produced by the flight tests.

Damping in yaw.- The results discussed thus far have been concerned with the unusual static yawing-moment characteristics of the configuration at zero sideslip. In addition to these characteristics, some unusual aerodynamic damping characteristics at spin attitudes were noted which were related to the moments produced by the nose of the airplane. Presented in figure 15 are the variations with angle of attack of the damping-in-yaw parameter $C_{n_r} - C_{n_{\dot{\beta}}} \cos \alpha$ and the side-force-due-to-yawing parameter $C_{Y_r} - C_{Y_{\dot{\beta}}} \cos \alpha$ measured for the 1/9-scale model at wing sweep angles of 26°, 50°,

and 72.5°. Negative values of $C_{n_r} - C_{n_{\dot{\beta}}} \cos \alpha$ are stabilizing (damping), whereas positive values are destabilizing (propelling in a spin). As can be seen, positive values of $C_{n_r} - C_{n_{\dot{\beta}}} \cos \alpha$ existed for angles of attack between about 50° and 70° for each wing-sweep angle. It should be noted that the positive values of $C_{n_r} - C_{n_{\dot{\beta}}} \cos \alpha$ are very large; for example, the magnitudes of the propelling moment due to rate of rotation at $\alpha = 57^\circ$ were about 10 times as large as the stabilizing values of damping in yaw at an angle of attack of 0°. These results indicate that the configuration would exhibit propelling values of yawing moment at high angles of attack; these yawing moments may produce autorotation.

An indication as to the airframe components producing the propelling moments can be obtained by analysis of the relationship of the yawing moment and side force acting on the airplane during a spin. Figure 16 shows a plan view of the airplane during a right spin. If the fuselage nose is producing the propelling moments due to yaw rate, a side force of the same sign as the yawing moment will exist. If the tail components are producing the propelling moments, the side force will have an opposite sign. An inspection of the data of figure 15 reveals that positive (side force to the right) values of $C_{Y_r} - C_{Y_{\dot{\beta}}} \cos \alpha$ accompanied the positive values of yawing moment due to yaw rate. If the effective center of pressure of this lateral force is calculated from the relation

$$\frac{x}{b} = \frac{C_{n_r} - C_{n_{\dot{\beta}}} \cos \alpha}{C_{Y_r} - C_{Y_{\dot{\beta}}} \cos \alpha}$$

it is found to be about halfway between the tip of the nose and the windshield. Based on the foregoing analysis, the nose of the configuration was primarily responsible for the propelling moments. Although the data are not presented, the results of forced-oscillation tests of the isolated fuselage were essentially the same as those of figure 15 for angles of attack greater than about 40°. This result also serves to verify the fact that the fuselage nose was producing the propelling moments.

Additional verification of the fact that the fuselage nose produced the propelling yawing moments was afforded by the results of static force tests which can be of considerable help in the analysis of the dynamic case. In such an analysis, the variations of C_n and C_Y with β are analyzed with consideration of the sideslip angle due to yawing rotation at the front and rear of the airplane. For example, the sideslip angle generated at the front of the airplane during a right spin is illustrated in figure 17. The sketch on the left-hand side of the figure shows the plan view of the airplane during a right spin with zero bank angle. The arrows along the fuselage nose indicate the relative magnitude and sense of the linear sideward velocities along the fuselage due to the

spinning rotation. The sketch on the right-hand side of the figure illustrates the sideslip angle at a typical nose location due to the spin rotation. As can be seen, the airplane rate of descent and the sideward velocity at the nose of the airplane combine vectorially to produce a positive sideslip angle β at the nose.

The fact that the nose of the configuration produced large yawing moments due to sideslip at high angles of attack was indicated by the results of static wind-tunnel tests to determine values of the static lateral-directional stability derivatives. Shown in figure 18 are the variations of the static stability derivatives C_{Y_β} and C_{n_β} with angle of attack for wing sweep angles of 26°, 50°, and 72.5°. The variation of C_{n_β} with α shows that the directional stability becomes negative, or unstable, for the various wing-sweep angles at angles of attack between 23° and 30°. As the angle of attack was increased above about 50°, the values of C_{n_β} became positive; and at an angle of attack of 60°, the value of C_{n_β} was about four times as large as the value at $\alpha = 0^\circ$. The large increase in directional stability was accompanied by a large positive change in C_{Y_β}, and indicated that the nose of the airplane was responsible for the large yawing moments due to sideslip just as it has been shown to be responsible for the positive (propelling) values of the damping-in-yaw derivative $C_{n_r} - C_{n_{\dot\beta}} \cos \alpha$. (The fact that long pointed bodies can produce positive side forces when subjected to positive angles of sideslip has been noted in past studies of entry bodies such as those of refs. 11 and 12.)

With the fact established that the nose of the fuselage was producing the trends shown for the yawing moment due to yawing velocity and the yawing moment due to sideslip, it is possible to make some deductions with regard to the linearity of C_n with r from the linearity of C_n with β. For example, shown in figure 19 is the variation of C_n with β for the present configuration at an angle of attack of 55°. Results are shown for the low Reynolds number tests conducted at the Langley Research Center and additional data are presented for tests conducted at a considerably higher Reynolds number at the Ames Research Center. With the concepts of figure 17 in mind, the data indicate that the basic configuration produced nose-right (propelling) yawing moments when subjected to positive angles of sideslip from 0° to about 25°, and nose-left (damping) moments at higher angles of sideslip. The characteristic S-shape of the C_n variation with β is apparently associated with the separation and attachment pattern of the vortex sheets shed off the nose. This result indicates that as the rate of spin due to the propelling moment increases (and results in larger values of effective sideslip angle at the nose), the propelling moment approaches zero. Thus, the variation of yawing moment with rate of yaw would be expected to be extremely nonlinear during a spin. The equilibrium condition implied by C_n being zero at $\beta = 23^\circ$ can be calculated by the relations:

$$\frac{rb}{2V} = \frac{\beta(\text{at nose})}{2\frac{x}{b}}$$

and

$$\frac{\Omega b}{2V} = \frac{\frac{rb}{2V}}{\sin \alpha}$$

and is found to be $\frac{\Omega b}{2V} = 0.61$. This value correlates reasonably well with the value of 0.70 which was measured in the single-degree-of-freedom autorotation tests which are discussed later. Such nonlinear trends of damping in yaw at high angles of attack have also been noted in past investigations. (See refs. 13 and 14.) Comparison of spin calculations with flight tests also indicated this nonlinearity of C_n with r since some calculations indicated an unrealistic continuous increase in spin rate due to positive values of $C_{n_r} - C_{n_{\dot{\beta}}} \cos \alpha$ whereas flight tests showed a finite spin rate. It therefore appears that adequate theoretical representation of yawing moments acting on the present configuration during a spin must take into account nonlinear variations of yawing moment with yaw rate.

Damping in pitch.- The model also exhibited unstable values of damping in pitch at high angles of attack. Shown in figure 20 is the variation of the aerodynamic damping-in-pitch parameter $C_{m_q} + C_{m_{\dot{\alpha}}}$ for the 1/9-scale model with a wing sweep of 50°. Negative values of this parameter denote stabilizing values, whereas positive values denote destabilizing values. The data indicate that positive values of $C_{m_q} + C_{m_{\dot{\alpha}}}$ were measured at high angles of attack. Inspection of the normal-force-due-to-pitching parameter $C_{N_q} + C_{N_{\dot{\alpha}}}$ did not produce any significant clues as to the airframe components producing the trends.

Effects of nose strakes.- The nose strakes tested in the investigation were designed either to control the sense of the large out-of-trim yawing moments created by the fuselage forebody and thereby enhance spin recovery, or to eliminate the propelling values of damping in yaw created by the nose. The single-strake configuration shown in figure 3(a) was found to be an effective means of controlling the sense of the out-of-trim yawing moments. Shown in figure 21 is the variation of C_n with α for zero sideslip for the configuration with the strake of figure 3(a) on the left side or the right side of the nose. The data show that the configuration with the strake on the left side exhibited nose-right out-of-trim moments, but, that when the strake was placed on the right side, the sense of the asymmetry changed, and a large nose-left moment asymmetry was produced. A

number of repeat tests indicated that the results obtained with the strake were consistent and repeatable.

The point to be inferred by the data presented in figure 21 is that a single strake could be used to produce consistently large yawing moments which might be used for spin recovery. It should be noted that the effectiveness of the strake in producing large yawing moments is considerably reduced at angles of attack greater than 70°; thus, it would not be expected to have an appreciable effect on a flat spin at higher angles of attack. This point should be kept in mind during subsequent sections of this paper.

The double-strake configuration shown in figure 3(b) eliminated the propelling tendencies of the nose. The effects of these strakes are shown in figure 22. This figure shows the variation of $C_{n_r} - C_{n_{\dot{\beta}}} \cos \alpha$ for the model with the double nose strakes on and off. The data show that these nose strakes eliminated the propelling tendencies of the nose and, in fact, added a substantial stabilizing contribution to the aerodynamic damping in yaw at angles of attack near 60°. It should be noted that the strakes had little effect at angles of attack greater than 75°. The effects of the double-strake arrangement on the variation of static yawing moment with sideslip is shown in figure 23. The data show the variation of C_n with β for the basic configuration and for the configuration with the strakes of figure 3(b) on the model. Addition of the strakes eliminated the propelling tendency of the nose by producing a linear variation of yawing moment with sideslip so that negative (damping) moments would be created by the nose in a right spin. It should be noted, however, that the large out-of-trim moment at $\beta = 0^{\circ}$ was not affected by the symmetrical strakes for this configuration. In addition, the data show that the strakes eliminated the large stable values of C_{n_β} exhibited by the basic configuration. This result should be kept in mind inasmuch as large changes in C_{n_β} may also affect spin characteristics.

The effects of these two strake configurations on the spin and recovery characteristics of the configuration were subsequently evaluated during autorotation tests and spin tests of dynamically scaled models.

Autorotation Tests

Single- and two-degree-of-freedom autorotation tests were conducted to verify some of the conclusions reached earlier concerning the asymmetric moments caused by the nose and the propelling tendencies of the nose. In addition, autorotative tendencies of the configuration with two degrees of freedom were studied to define the form of aerodynamic inputs necessary to calculate spins. It should be kept in mind that the autorotation tests were conducted for $\beta = 0^{\circ}$. Past experience has shown that angles of sideslip can have significant effects on airplane spin characteristics. Because of this

limitation and other considerations, the results of the autorotation tests must be interpreted cautiously for extrapolation to actual spins involving complete freedom of the airplane. Elimination of autorotative characteristics using this test technique should not therefore be viewed as a sufficient condition for spin prevention, but the test technique should be viewed as a means to identify conditions for which spins might readily occur because of the autorotative tendencies of the vehicle.

During the single-degree-of-freedom tests, the angle-of-attack pivot of the 1/10-scale model was locked and the model was allowed to rotate about the spin axis at various fixed angles of attack. The model was ballasted so that the center of gravity coincided at all times with the spin axis. Initial autorotation tests showed that the model would spin in one direction and not the other because of the out-of-trim yawing moments discussed earlier. A small piece of modeling clay (about 1/4-inch cube) was then placed on the tip of the nose and flattened slightly on the side of the nose toward which the model tended to spin. By thus slightly reshaping the nose, it was possible to obtain autorotation at the same rate of spin both to the right and to the left. The results of the single-degree-of-freedom tests with the nose-tip modification are shown in figure 24 as the variation of nondimensional spin rate $\Omega b/2V$ with angle of attack. The test results show that the model would autorotate at angles of attack between 50° and 75° as would be expected, based on the forced-oscillation data of figure 15. When disturbed from rest, the model would speed up to the nondimensional spin rates indicated in figure 24 and stabilize; when prerotated to spin rates faster than those indicated, the model would slow down to the indicated value of $\Omega b/2V$. When the nose was completely removed from the model (representing removal of the radome on the full-scale airplane), autorotation was eliminated over the entire angle-of-attack range.

These results verified the fact that the nose produced a propelling moment due to rate of spin in the 50° to 75° angle-of-attack range. In addition, the results established that the yawing moment was a nonlinear function of rate of rotation as deduced earlier from the variations of C_n with β, as was previously mentioned. The nondimensional rates of spin shown in figure 24 attained extremely large values, particularly near an angle of attack of 60°.

The two-degree-of-freedom tests in which the model was free to rotate about both the spin axis and the Y body axis were made to evaluate further the significance of the autorotational motions obtained during the single-degree-of-freedom tests. For example, if the autorotational spin rates produced by the nose were not sufficiently large during the two-degree-of-freedom tests, the model would pitch down and terminate autorotation because of the existence of a nose-down aerodynamic pitching moment at high angles of attack.

As illustrated in figure 25, the steady developed spin requires a balance between the aerodynamic moments and the inertial moments acting on the airplane. The sketch on the left of figure 25 shows that at spin attitudes, an airplane usually experiences a nose-down aerodynamic pitching moment. This aerodynamic pitching moment is balanced by the nose-up inertial moments depicted in the sketch at the right of the figure. In this right-hand sketch, the mass distribution of the airplane has been represented by a system of weights. As the weights rotate about the spin axis, centrifugal forces acting perpendicular to the spin axis create a nose-up inertial pitching moment; and for the steady developed spin, the nose-up inertial moment balances the nose-down aerodynamic moment. The magnitude of the inertial moment may be calculated by the expression:

$$C_{m,i} = 4\left(\frac{I_Z - I_X}{mb^2}\right)\left(\frac{\Omega b}{2V}\right)^2\left(\frac{b}{\bar{c}}\right)\mu_b \sin 2\alpha$$

The magnitude of the inertial moment is thus dependent on the inertial distribution of the airplane, the nondimensional spin rate, the relative density of the airplane, and the angle of attack. This expression has been used to calculate the magnitude of the inertial pitching moment for the present configuration based on typical mass characteristics for the configuration and the nondimensional spin rates obtained during the single-degree-of-freedom autorotation tests. Figure 26 presents the variation with angle of attack of this calculated inertial pitching moment (plotted with algebraic sign reversed) for sea-level conditions. The figure also presents the variation with angle of attack of the aerodynamic pitching moment as measured during static force tests. Points at which the two curves intersect denote potential steady spin calculations satisfying the condition of a balance of inertial and aerodynamic moments. As can be seen, two intersection points, denoted A and B, exist. Examination of the characteristics at point A, however, show this point to be an unstable equilibrium condition inasmuch as a positive increment of angle of attack at point A creates a larger nose-up inertial moment; therefore, the angle of attack will continue to increase until the stable conditions of point B are reached. Based on these data, the model when allowed two degrees of freedom would be expected to exhibit a steady spin at an angle of attack of 74° with a nondimensional spin rate of 0.25.

The results of the two-degree-of-freedom autorotation tests indicated that the model would not spin steadily at an angle of attack of 74°, but rather performed a periodic oscillatory spin in which the angle of attack oscillated between 60° and 85°. The oscillatory characteristics are believed to be related to the damping-in-pitch trends shown in figure 20. Unfortunately, an insufficient number of data points are available to enable

precise definition of data trends in the angle-of-attack region associated with the destabilizing values of $C_{m_q} + C_{m_{\dot{\alpha}}}$. Based on the trends shown, however, it appears that the potential steady spin angle of attack of 74° may have been accompanied by destabilizing values of $C_{m_q} + C_{m_{\dot{\alpha}}}$ which, when coupled with the single-degree-of-freedom autorotation characteristics, produced a limit-cycle motion. These two-degree-of-freedom results are considered to be very significant inasmuch as the results indicate that a realistic mathematical description of the aerodynamic characteristics of the present configuration during a spin will involve: (1) representation of the nonlinear variation of yawing moment with spin rate as exhibited by the model during the single-degree-of-freedom tests and (2) consideration of aerodynamic damping in pitch, and perhaps roll. These results suggest that a mathematical approach which combines aerodynamic data measured at various rates of spin with linearized damping derivatives (such as that used in ref. 15) will be the most realistic manner to represent aerodynamic characteristics of the vehicle during spins.

The effectiveness of the two nose strake configurations was also evaluated during the autorotation tests. With either the single- or double-strake configuration on the model, autorotation was eliminated during the single-degree-of-freedom tests. When the model was prerotated during the two-degree-of-freedom tests, it immediately slowed down, pitched nose down, and ceased rotation. It is believed that the single-strake configuration prevented autorotation by creating a large asymmetric yawing moment which opposed the spin. On the other hand, the double-strake configuration prevented autorotation by eliminating the propelling values of $C_{n_r} - C_{n_{\dot{\beta}}} \cos \alpha$ exhibited by the basic configuration at high angles of attack.

Spin-Tunnel and Outdoor Spin Tests

A limited number of spin-tunnel and outdoor radio-controlled spin tests were conducted to assess the importance of the fuselage nose on spin characteristics and to verify the effectiveness of the various nose strake configurations. The preceding analysis was based on limited degrees of freedom; of course, this condition is not true for the actual spin. Such factors as aerodynamic pitching moment and sideslip angle are known to affect spin characteristics to a considerable extent, and yawing-moment characteristics are but one of many factors influencing the spin. Hence, a true evaluation of the relative importance of the fuselage nose must come from actual spin tests.

Spin-tunnel tests.- The spin-tunnel tests included tests of the basic configuration, and tests to determine the effects of single- and double-strake arrangements. In order to produce more consistent and critical spins to the left, a small flat spot was created on the right-hand side of the nose of the model. The more consistent results obtained with

the modified nose are probably attributable to the asymmetric moment created by the flat spot as indicated by the data of figure 13. The nose-left yawing moment produced by the nose increased the tendency of the model to spin to the left. The results obtained for the basic configuration and the effects of the single-strake arrangements of figure 6 are listed in table II.

The results of the spin-tunnel tests for the limited mass loadings and control positions investigated showed that the model exhibited a fast-flat spin at an angle of attack of about 82°. The flat spin was repeatable and was obtained during several check tests. Recoveries from the developed flat spin were considered to be unsatisfactory $\left(\text{number of turns for recovery} > 2\frac{1}{4}\right)$. After application of recovery controls, the model would begin to recover from the flat spin; however, after the angle of attack had diminished to about 75°, the model entered an oscillatory-spin mode which required several additional turns for recovery.

Initial attempts at evaluating the effects of the fuselage forebody on spin characteristics consisted of ejection of the entire nose (simulating ejection of the radome) during the developed spin. These tests, the results of which are not presented in table II, showed that the model continued to spin flat after ejection of the nose. This result indicates that other factors, such as aerodynamic pitching moment and wing tilt (angles of sideslip) were more important factors than the nose insofar as the characteristics of the developed flat spin were concerned. The earlier autorotation tests with two degrees of freedom had indicated that autorotation would cease when the radome was ejected; but the model was not in a flat spin in the autorotation tests. Both the fact that the model would not spin flat in the autorotation tests at zero sideslip and the fact that the autorotation tests indicated that the model would not spin with the radome removed serve to stress the limitations of autorotation tests and the importance of sideslip on spin characteristics.

A limited number of tests were conducted to determine the effects of the extended double strakes of figure 3(b) on spin characteristics. These strakes, which were designed to eliminate the unstable values of damping in yaw shown in figure 15, were found to have virtually no effect on the developed flat spin. This result might be expected inasmuch as the data presented in figure 22 show little effect of the strakes above an angle of attack of 75°. It should be pointed out, however, that in isolated cases when the developed flat spin finally degenerated into an oscillatory-type spin involving the lower angles of attack at which the strakes were more effective, the spin rate appeared to cease within one turn after the angle of attack had diminished to 60° or 70°, and the model dived out of the spin.

A series of tests were also conducted to evaluate various single-strake arrangements as possible recovery controls. The data of table II show that when a strake was placed on the left side of the nose of the model in an extended position, the model still

exhibited a flat spin. This result might be expected based on the data of figure 21 which shows that the strake was relatively ineffective at angles of attack above 80°. However, when recovery from the developed spin was attempted by using the recommended recovery control technique, the recoveries were rapid and consistent in contrast to the slow recoveries for the basic configuration. The extended single strake did not, therefore, prevent a flat spin when the model was launched into the spin at an angle of attack near 90°, but the strake did provide satisfactory recoveries when used in conjunction with application of the conventional recovery controls. The results of the tests with strakes 2 to 5 indicated generally similar results, although a slight increase in the number of turns for recovery was noted when the strake was reduced in length or removed from the tip of the nose. Satisfactory recoveries were effected from the flat spin with the single-strake arrangements which did not directly affect the characteristics of the developed fast-flat spin because as the angle of attack diminished slightly, the strakes became effective in producing antispin asymmetric yawing moments as indicated by figure 21.

One additional test made during the program was the actual extension of a single strake after the developed fast-flat spin was established. When strake 6 (see fig. 6) was extended during a flat spin, together with simultaneous deflections of the conventional control surfaces, recoveries were less rapid than when the strake was extended before recovery controls were applied and were unsatisfactory. When only the strake was used for recovery (with the conventional control surfaces maintained at pro-spin deflections), no recoveries from the flat spin were achieved.

Based on the results of these limited tests, it appears that a single-strake configuration may improve the spin-recovery characteristics of the present configuration but the strake must be extended relatively early in the incipient spin stage before the flat spin is allowed to develop. In this way, it would be extended in the 40° to 70° angle-of-attack range where it is very effective, and the flat spin might not ever develop.

Outdoor spin tests.- The results of the outdoor free-flight tests showed that the present configuration was prone to be in a developed flat spin within two turns after departure from controlled flight. It was believed that addition of the double-strake arrangement of figure 3(b) might negate any contribution of the unstable values of damping in yaw to spin entry, and that this lack of a propelling yawing moment might prevent the configuration from entering the developed flat spin.

The results of four flights showed that with strakes on the nose, stall characteristics appeared to be relatively similar to the basic configuration; that is, an incipient spin was produced by applying full back stick with neutral lateral controls. The nature of the incipient and developed spin, however, was different when strakes were employed. With nose strakes, the model exhibited an oscillatory flat spin from which recovery was rapid by using conventional recovery techniques; whereas the basic configuration exhibited a

fast-flat spin with no recovery. The results also indicated that full pro-spin controls were required to maintain a spin with the strakes installed on the model.

SUMMARY OF RESULTS

An investigation to determine the effects of a pointed fuselage nose on the spin characteristics of a fighter airplane model has produced the following results:

1. Theoretical calculations of the spin characteristics of the model did not correlate with results obtained during free-flight tests of the model because of large, random asymmetric yawing moments at high angles of attack.

2. The large asymmetric moments were produced by flow separation off the long pointed nose of the configuration at high angles of attack. The sense of the asymmetric moment was established by slight geometric or aerodynamic asymmetries and could be controlled by a nose strake located on one side of the nose.

3. The nose of the configuration produced large propelling values of the aerodynamic damping-in-yaw parameter $C_{n_r} - C_{n_{\dot{\beta}}} \cos \alpha$ at high angles of attack which promoted autorotational tendencies.

4. The nose strake did not eliminate a flat spin exhibited by the configuration, but substantial improvement in recovery from the developed flat spin was noted.

5. To be most effective as spin-recovery devices for the present configuration, nose strakes should be deployed soon after the stall and loss of control, and before the flat spin developed.

Langley Research Center,
National Aeronautics and Space Administration,
Hampton, Va., July 2, 1970.

REFERENCES

1. Neihouse, Anshal I.; Klinar, Walter J.; and Scher, Stanley H.: Status of Spin Research for Recent Airplane Designs. NASA TR R-57, 1960. (Supersedes NACA RM L57F12.)

2. Chambers, Joseph R.; and Grafton, Sue B.: Static and Dynamic Longitudinal Stability Derivatives of a Powered 1/9-Scale Model of a Tilt-Wing V/STOL Transport. NASA TN D-3591, 1966.

3. Libbey, Charles E.; and Burk, Sanger M., Jr.: A Technique Utilizing Free-Flying Radio-Controlled Models To Study the Incipient- and Developed-Spin Characteristics of Airplanes. NASA MEMO 2-6-59L, 1959.

4. Letko, William: A Low-Speed Experimental Study of the Directional Characteristics of a Sharp-Nosed Fuselage Through a Large Angle-of-Attack Range at Zero Angle of Sideslip. NACA TN 2911, 1953.

5. Spence, A.; and Trebble, W. J. G.: Low Speed Tunnel Tests on the Flow Structure Behind a Body of Revolution of Fineness Ratio 16 2/3:1. Tech. Note No. Aero. 2406, Brit. R.A.E., Oct. 1955.

6. Fink, P. T.; and Taylor, J.: Some Early Experiments on Vortex Separation. R. & M. No. 3489, Brit. A.R.C., 1967.

7. Ferris, James C.: Static Stability Investigation of a Single-Stage Sounding Rocket at Mach Numbers From 0.60 to 1.20. NASA TN D-4013, 1967.

8. Dunn, Eldon L.: A Low-Speed Experimental Study of Yaw Forces on Bodies of Revolution at Large Angles of Pitch and Zero Angle of Sideslip. TM-1588, U.S. Naval Ord. Test Station, Mar. 8, 1954.

9. Shanks, Robert E.: Low-Subsonic Measurements of Static and Dynamic Stability Derivatives of Six Flat-Plate Wings Having Leading-Edge Sweep Angles of 70° to 84°. NASA TN D-1822, 1963.

10. Boisseau, Peter C.: Low-Subsonic Static Stability and Damping Derivatives at Angles of Attack From 0° to 90° for a Model With a Low-Aspect-Ratio Unswept Wing and Two Different Fuselage Forebodies. NASA MEMO 1-22-59L, 1959.

11. Spencer, Bernard, Jr.; and Phillips, W. Pelham: Effects of Cross-Section Shape on the Low-Speed Aerodynamic Characteristics of a Low-Wave-Drag Hypersonic Body. NASA TN D-1963, 1963.

12. Spencer, Bernard, Jr.; and Phillips, W. Pelham: Transonic Aerodynamic Characteristics of a Series of Bodies Having Variations in Fineness Ratio and Cross-Sectional Ellipticity. NASA TN D-2622, 1965.

13. Scherer, Michel; and Louis, Bernard: Étude Analytique de la Vrille. O.N.E.R.A. T.P. No. 187, 1964.

14. Chambers, Joseph R.; Bowman, James S., Jr.; and Anglin, Ernie L.: Analysis of the Flat-Spin Characteristics of a Twin-Jet Swept-Wing Fighter Airplane. NASA TN D-5409, 1969.

15. Anglin, Ernie L.; and Scher, Stanley H.: Analytical Study of Aircraft-Developed Spins and Determination of Moments Required For Satisfactory Spin Recovery. NASA TN D-2181, 1964.

TABLE I.- DIMENSIONAL CHARACTERISTICS OF THE AIRPLANE

[All dimensions are based on 16° wing sweep]

Overall length	882.1 in. (2240.5 cm)
Wing:	
Span	63 ft (19.2 m)
Area	525 ft^2 (48.8 m^2)
Root chord (at airplane center line)	150.883 in. (383.2 cm)
Tip chord	49 in. (124.5 cm)
Mean aerodynamic chord, $\bar{c}$	108.5 in. (275.6 cm)
Leading edge of $\bar{c}$, rearward of leading edge of root chord	45 in. (114.3 cm)
Aspect ratio	7.56
Taper ratio	3.08
Dihedral	1°
Incidence	1°
Airfoil section:	
Root	NASA 64A210.68 (modified)
Tip	NASA 64A209.8 (modified)
Horizontal tail:	
Total area	407.3 ft^2 (37.8 m^2)
Span	29.33 ft (8.94 m)
Aspect ratio	2.11
Taper ratio	6.897
Sweepback of leading edge	57°30'
Dihedral	-1°
Root chord (at airplane center line)	269 in. (683.26 cm)
Tip chord (theoretical)	39 in. (99.06 cm)
Airfoil section	Biconvex
Vertical tail:	
Area	111.7 ft^2 (10.4 m^2)
Span	8.9 ft (2.7 m)
Taper ratio	2.435
Root chord	213.47 in. (542.2 cm)
Tip chord	87.67 in. (222.7 cm)
Sweepback of leading edge	55°
Airfoil section	Biconvex
Rudder area	29.3 ft^2 (2.72 m^2)

TABLE I.- DIMENSIONAL CHARACTERISTICS OF THE AIRPLANE – Concluded

Dimensions for other wing sweep angles:				
Wing sweep angle	16°	26°	50°	72.5°
Span, ft (m)	63 (19.2)	59.5 (18.1)	48.3 (14.7)	31.95 (9.74)
Mean aerodynamic chord, $\bar{c}$, in. (cm)	108.5 (275.6)	109.8 (278.9)	143.6 (364.7)	277.48 (704.8)
Leading edge $\bar{c}$ fuselage station, in. (cm)	478.0 (1214.1)	489.0 (1242.1)	489.6 (1243.6)	380.6 (966.7)

TABLE II.- RESULTS OF SPIN-TUNNEL TESTS

[Recovery attempted from and developed spin data presented for rudder full with spins; left erect spins; model values converted for full-scale values]

Strake	Developed spin characteristics		Control movement for recovery (a)			Turns for recovery
	Ω, rps	α, deg	Elevator	Ailerons	Rudder	
Basic configuration						
	0.38	82	25U	8W	7.5A	$10\frac{1}{4}, 6\frac{1}{2}, 4, 4\frac{1}{2}$
Extended strake on left side						
1	0.32	80	25U	8W	7.5A	$1\frac{1}{2}, 1$
2	.35	81	25U	8W	7.5A	$1\frac{1}{2}, 2$
3	.36	81	25U	8W	7.5A	$2, 2\frac{1}{2}$
4	.37	82	25U	8W	7.5A	$2, 2\frac{1}{2}$
5	.36	82	25U	8W	7.5A	$1\frac{3}{4}, 2\frac{1}{2}$
Strake extended during developed spin						
6	0.39	83	25U	8W	7.5A	$3, 3\frac{3}{4}$
[b]6			0	8A	7.5W	∞, ∞

[a]A, against; W, with; U, trailing edge up.

[b]Recovery attempted by strake only.

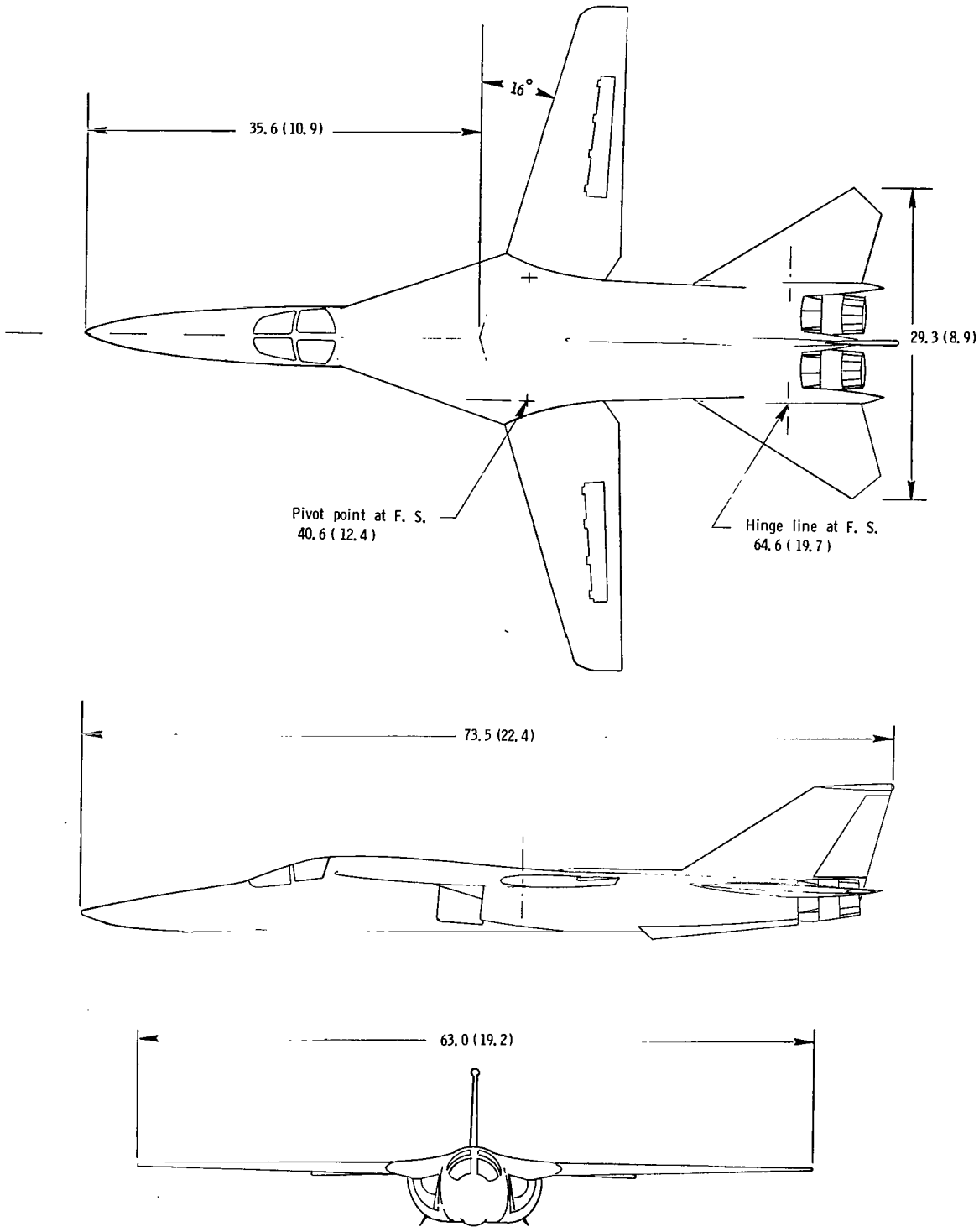

Figure 1.- Three-view sketch of airplane configuration. Dimensions are in feet (meters).

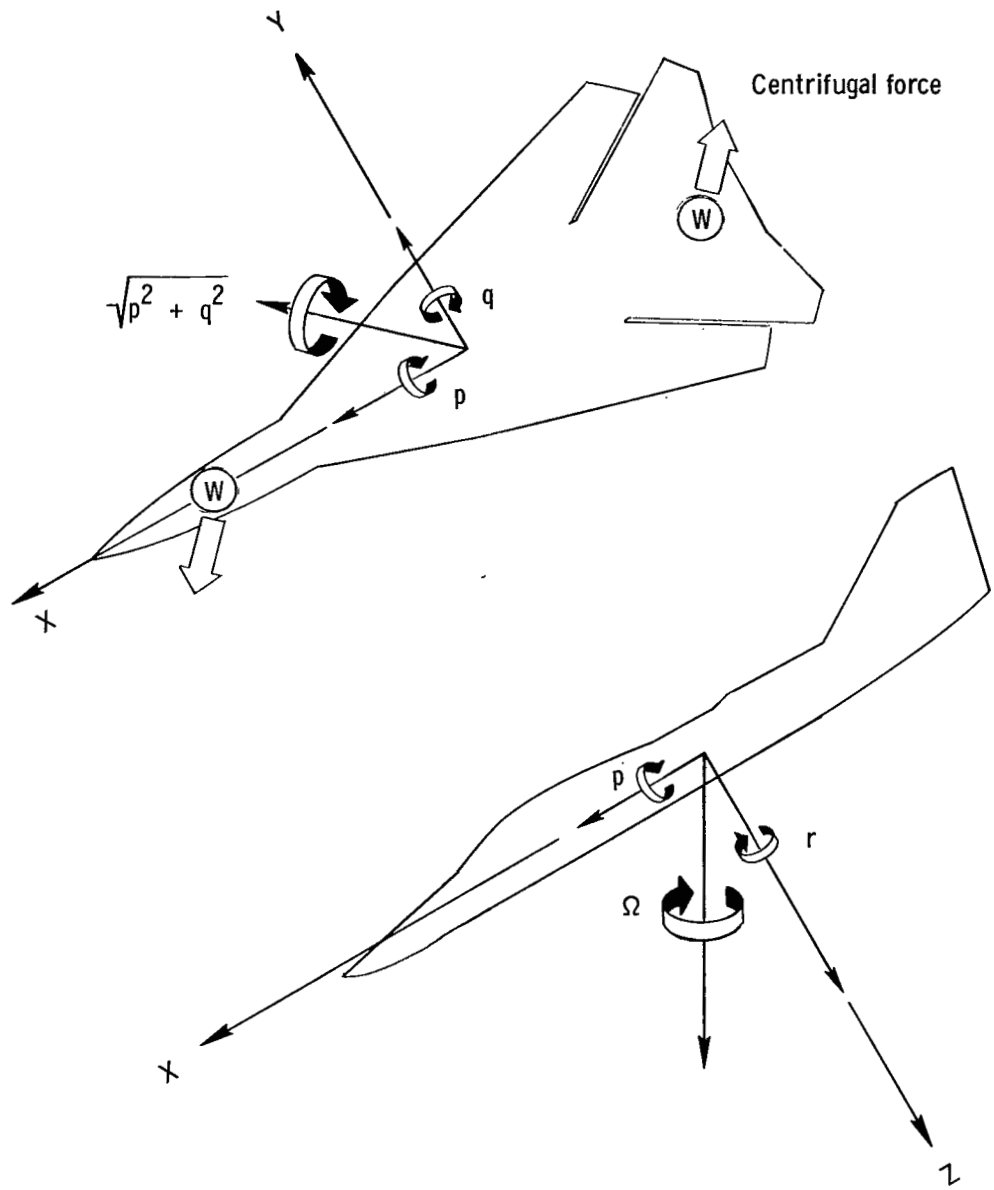

Figure 2.- Sketch illustrating mechanism by which gyroscopic antispin moment is produced.

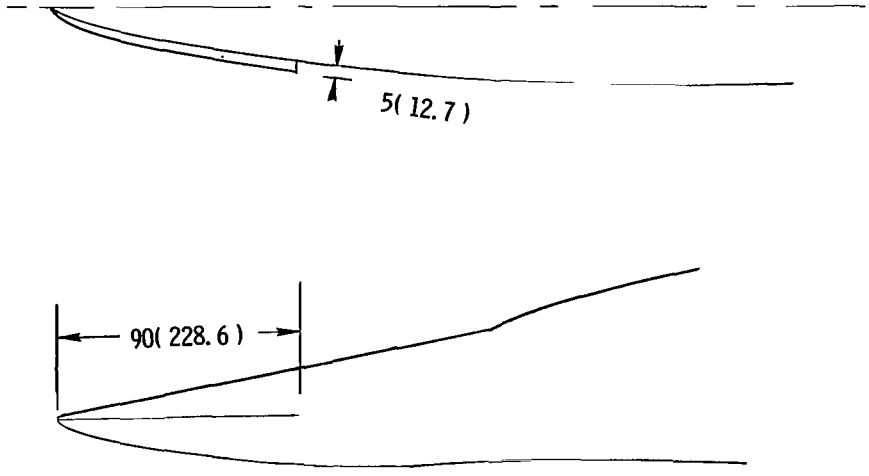

(a) Single-strake arrangement.

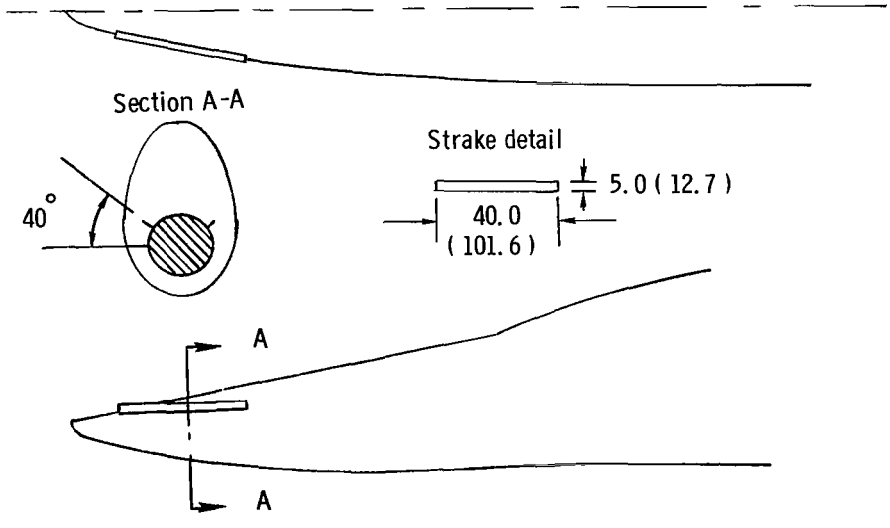

(b) Double-strake arrangement.

Figure 3.- Strake arrangements studied during force tests. Dimensions are full scale and are given in inches (centimeters).

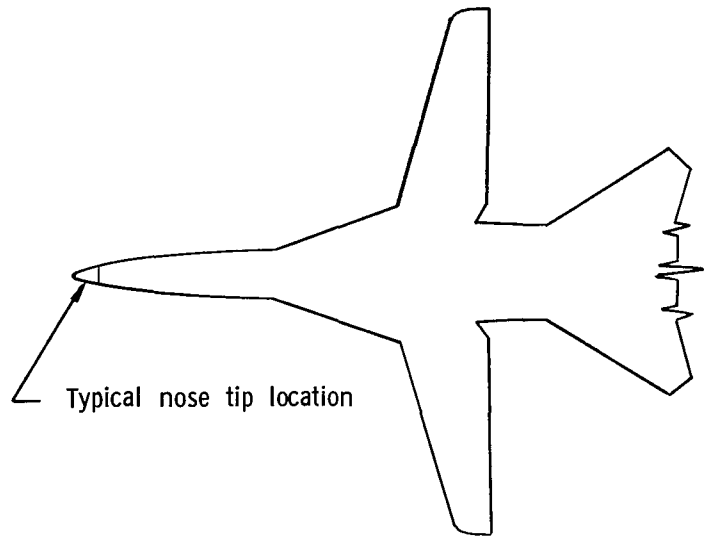

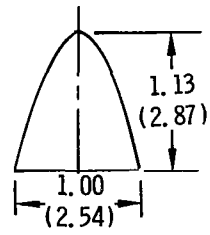

Basic nose tip

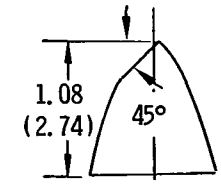

Basic tip with small flat on left side (or right side)

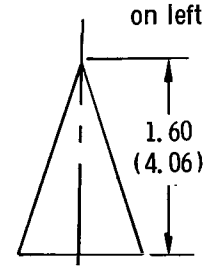

Pointed nose tip

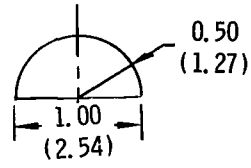

Plan view

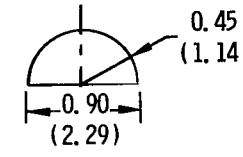

Side view

Rounded nose tip

Figure 4.- Plan view of fuselage nose tips studied during force tests. Dimensions are in inches (centimeters) and are given for 1/15-scale model.

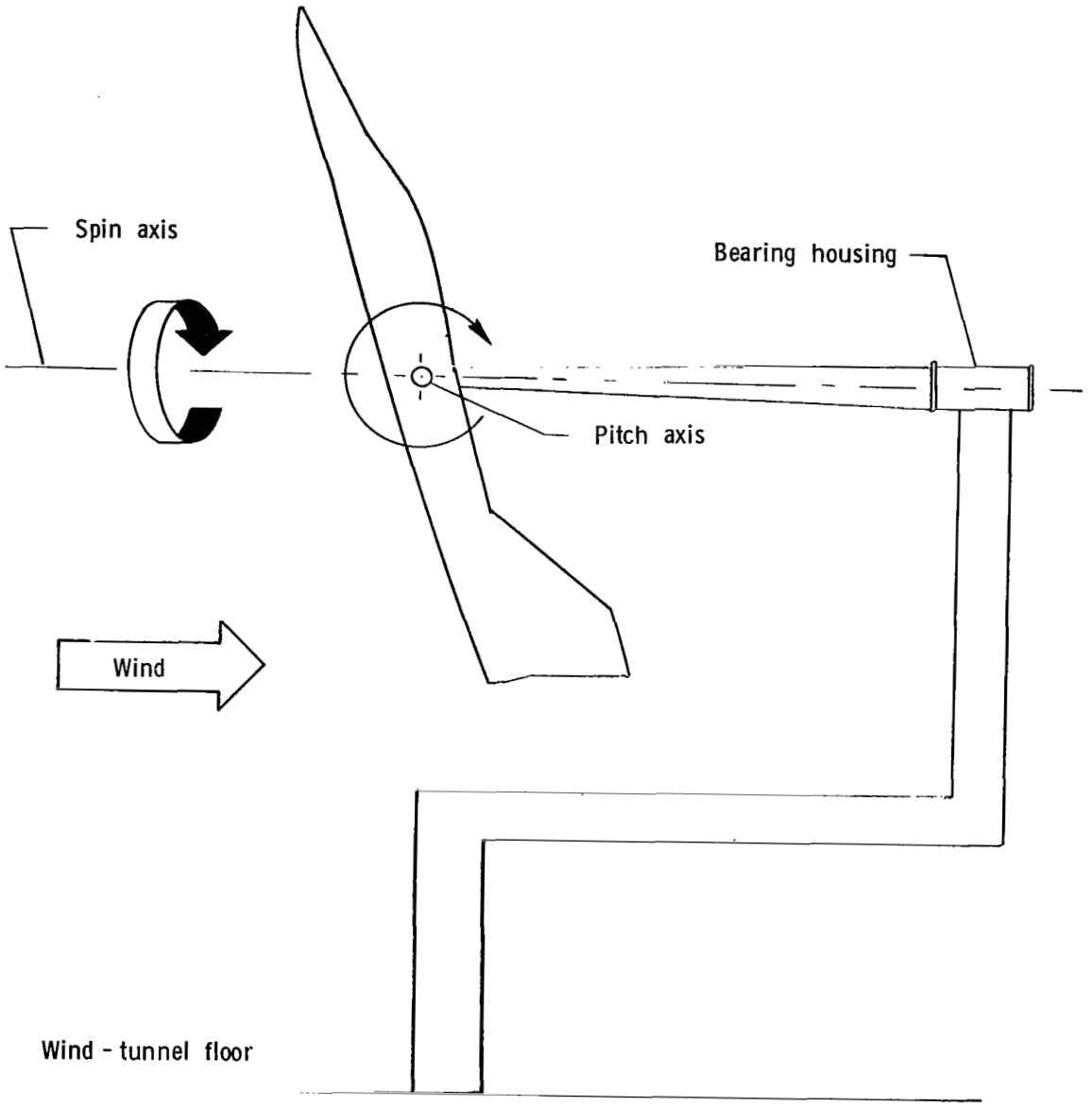

Figure 5.- Sketch of test setup for autorotation tests.

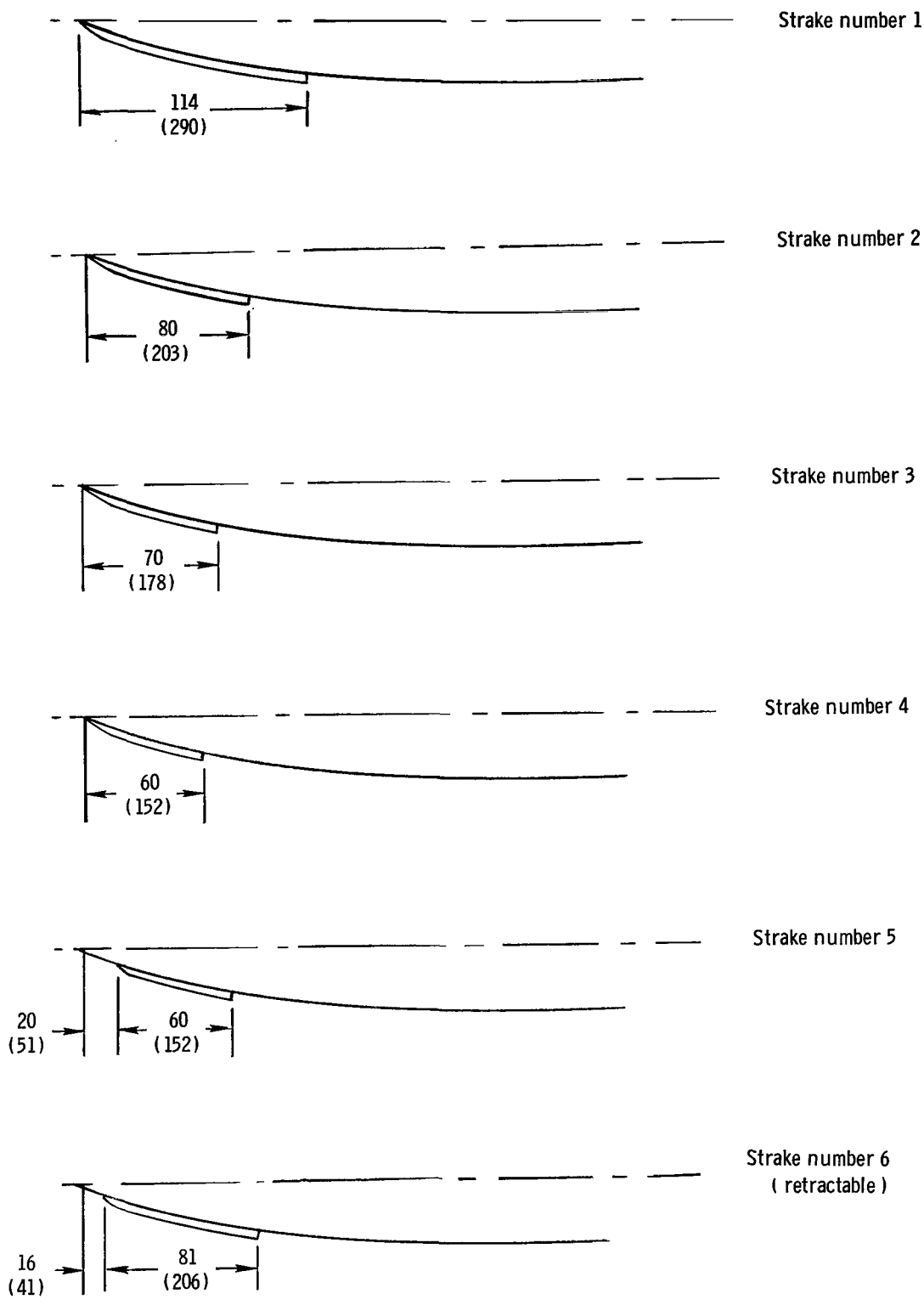

Figure 6.- Plan views of nose-strake configurations studied during spin-tunnel tests. Strakes were placed on left-hand side of nose. Dimensions are full scale and are given in inches (centimeters).

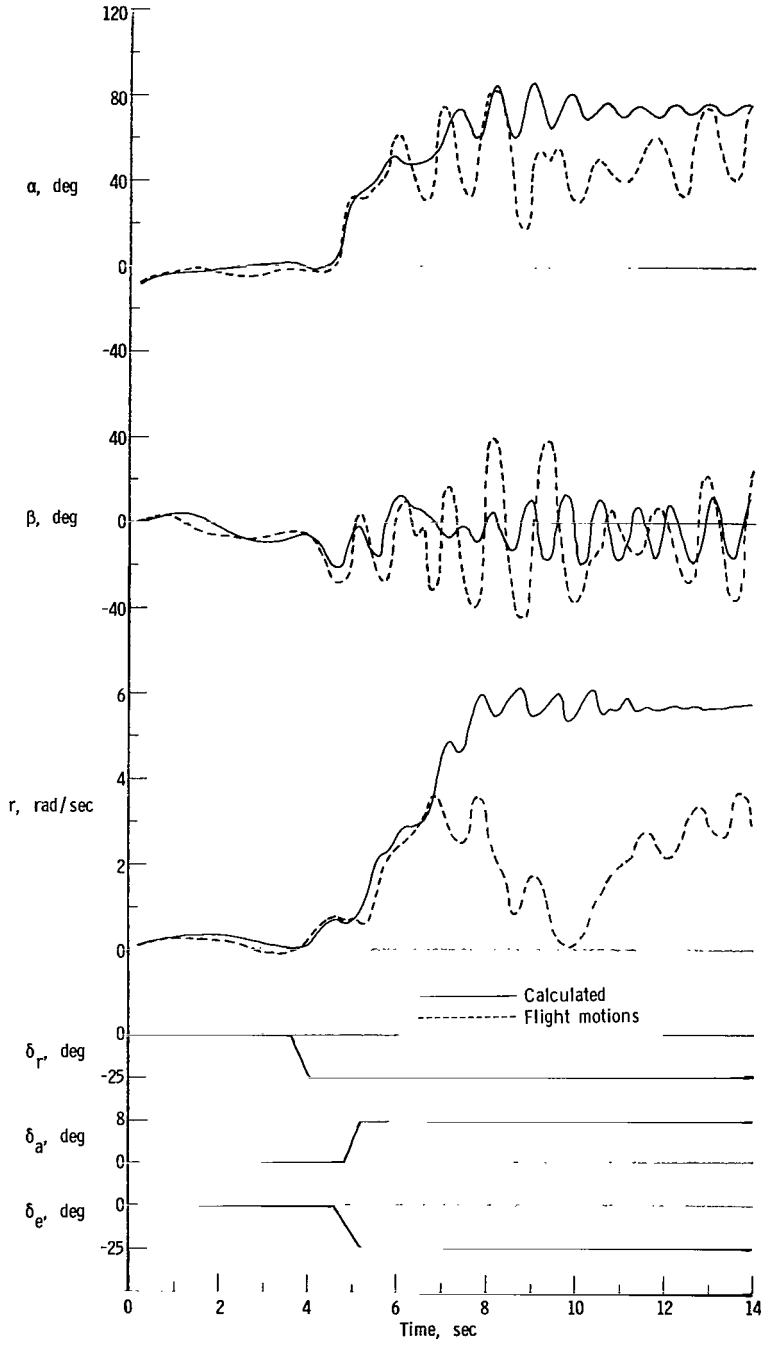

(a) Flight 1.

Figure 7.- Comparison of theoretical spin calculations and free-flight model motions for identical control inputs. $\Lambda = 50^{\circ}$; time given in model scale.

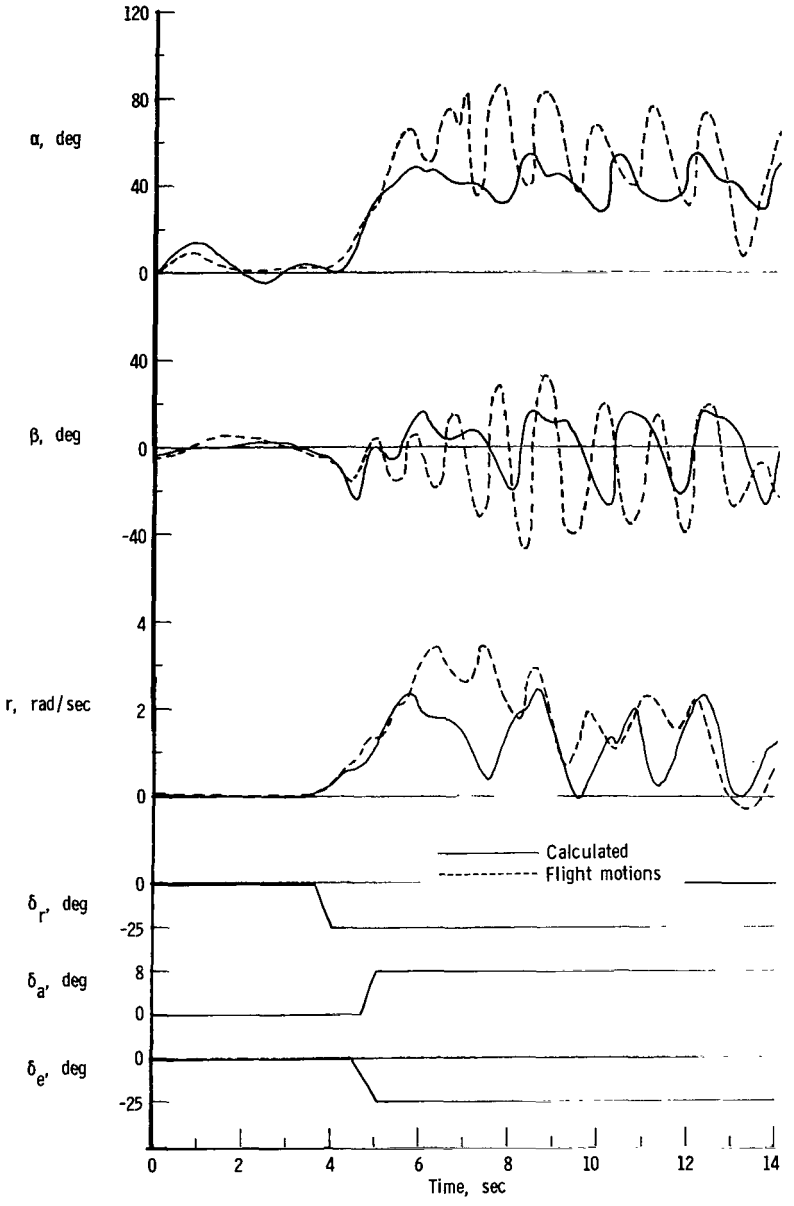

(b) Flight 2.

Figure 7.- Continued.

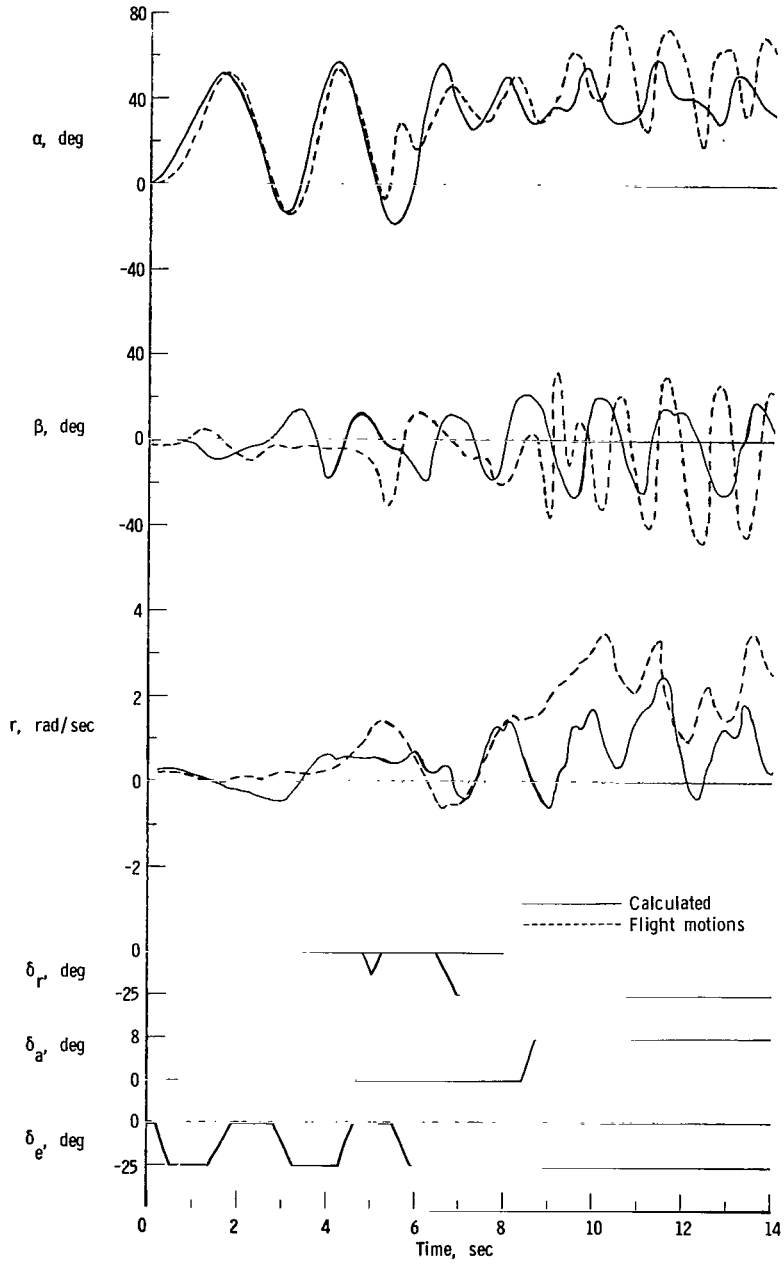

(c) Flight 3.

Figure 7.- Concluded.

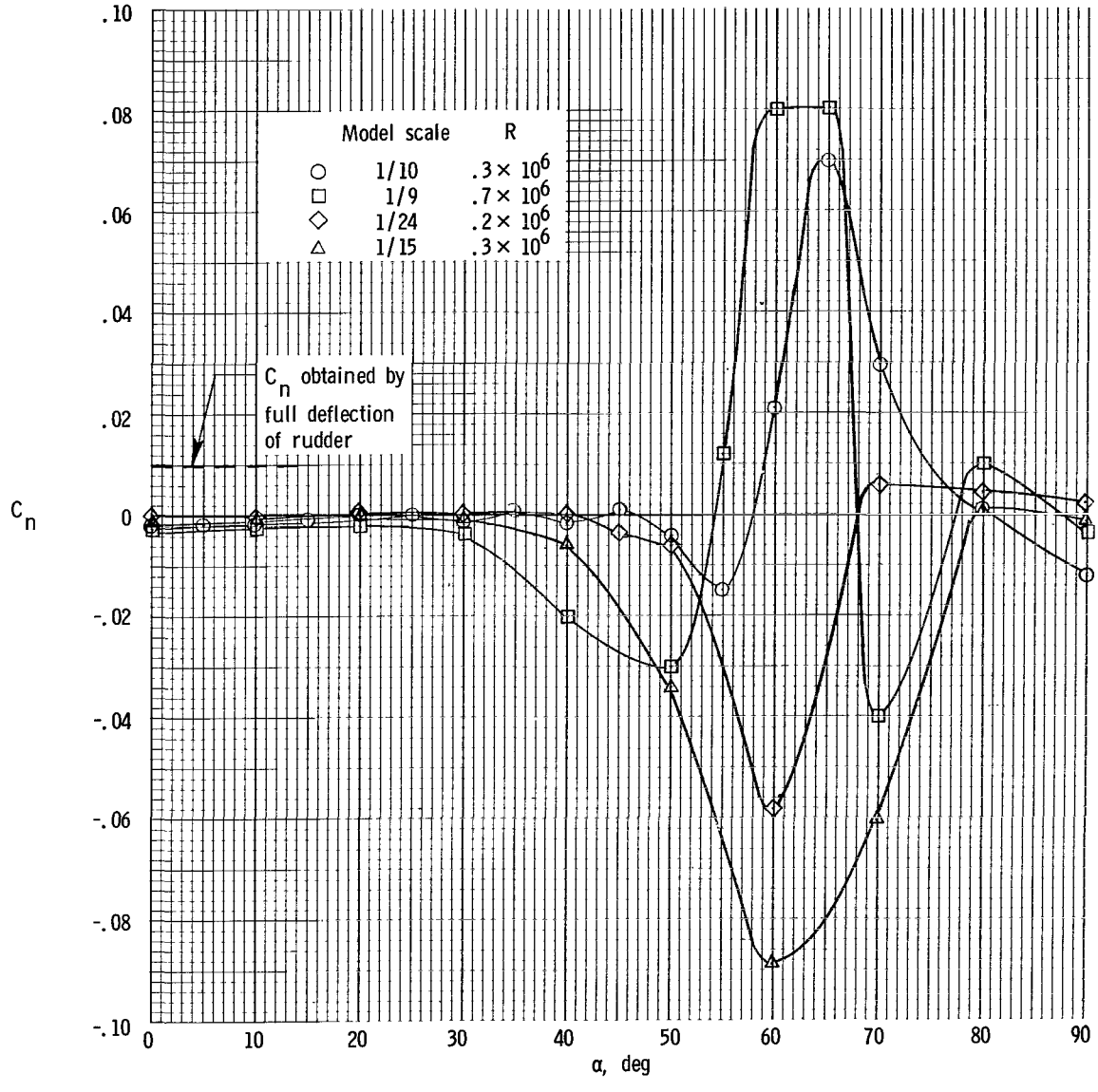

Figure 8.- Variation of static yawing-moment coefficient with angle of attack for several models of the present configuration. $\beta = 0^{\circ}$; $\Lambda = 50^{\circ}$; $\delta_r = 7.5^{\circ}$.

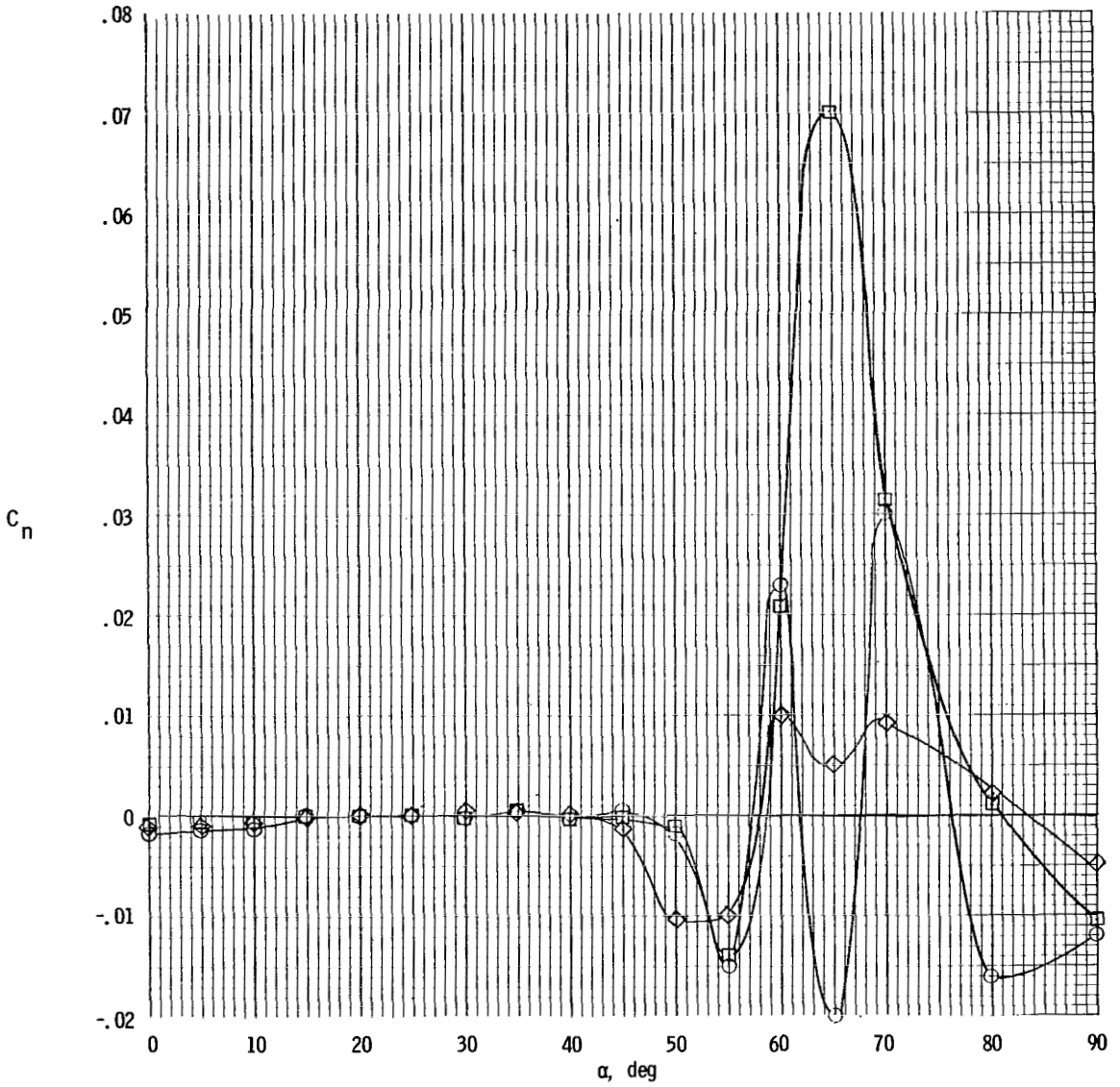

Figure 9.- Variation of yawing-moment coefficient with angle of attack. Symbols indicate values obtained in several repeat tests. $\Lambda = 50^{\circ}$; $\beta = 0^{\circ}$; $\delta_e = \delta_a = \delta_r = 0^{\circ}$; $R = 0.3 \times 10^6$.

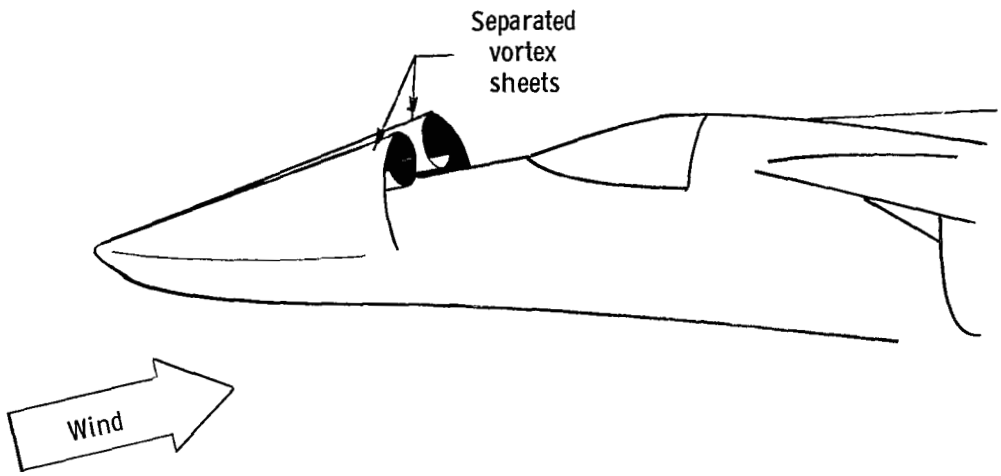

(a) Low angles of attack.

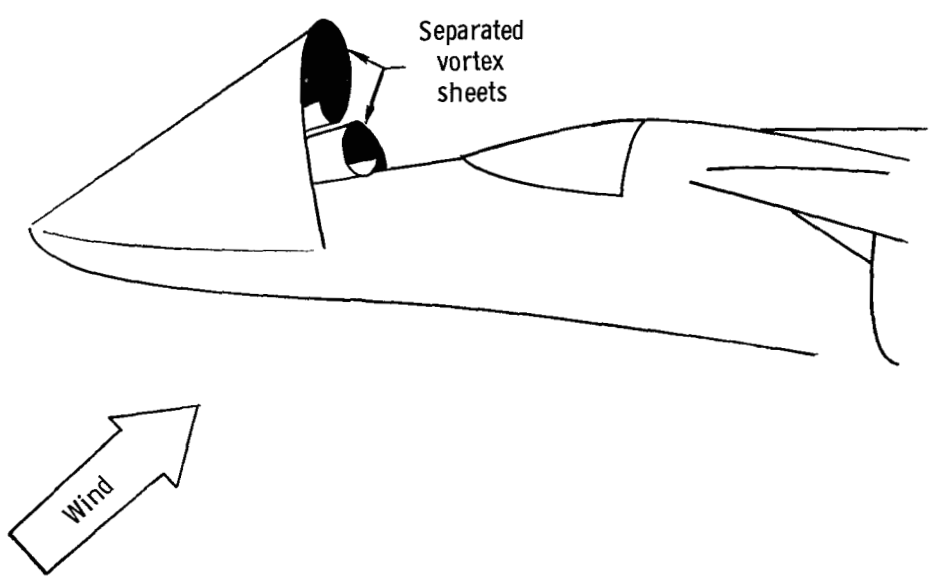

(b) High angles of attack.

Figure 10.- Sketches of separated vortex sheets on fuselage forebody.

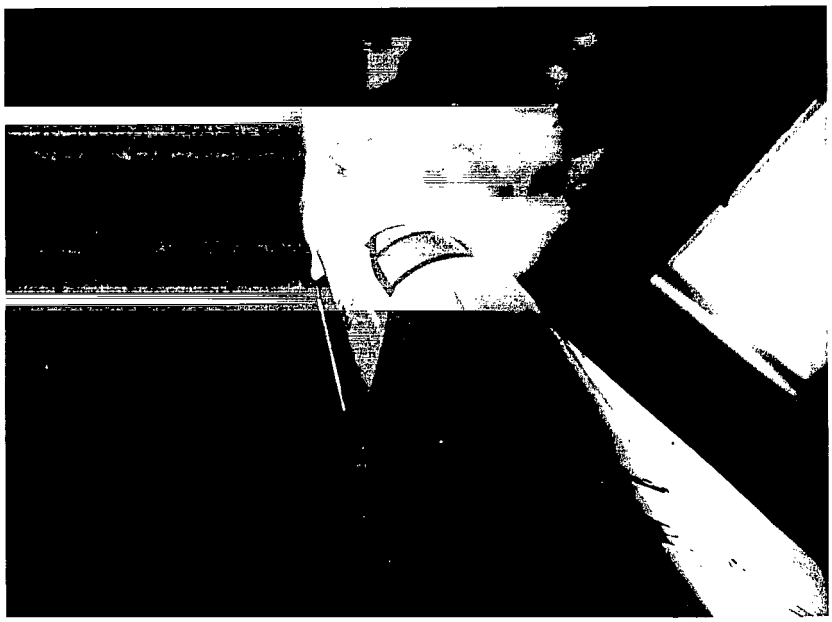

L-70-4705

(a) Three-quarter rear view.

L-70-4706

(b) Side view.

Figure 11.- Typical smoke pattern about fuselage forebody of $\frac{1}{10}$-scale model. $\alpha = 60^{\circ}$; $\beta = 0^{\circ}$; $\Lambda = 50^{\circ}$; $R = 0.3 \times 10^{6}$.

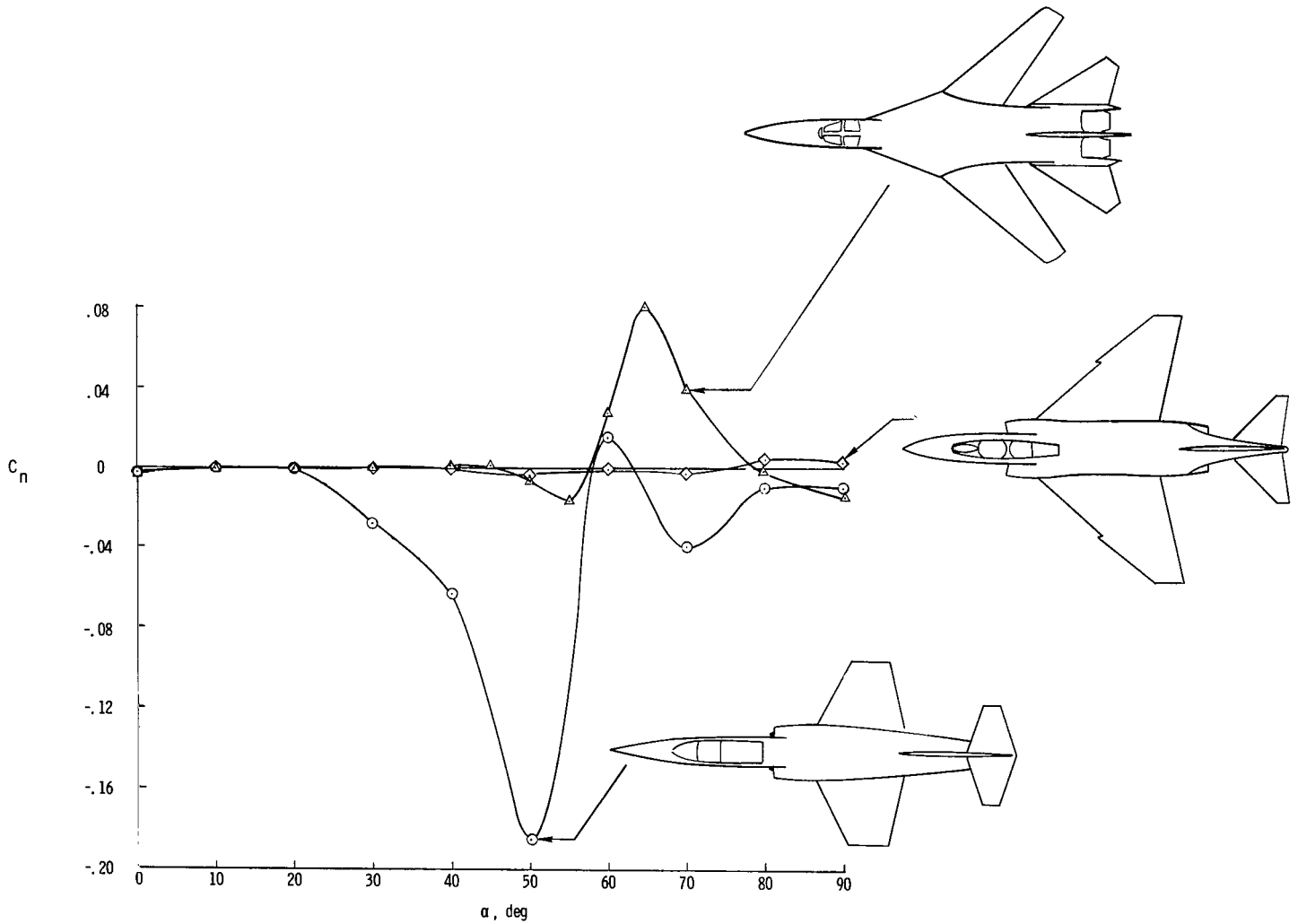

Figure 12.- Variation of yawing-moment coefficient with angle of attack for several airplane configurations. $\beta = 0^{\circ}$; $R = 0.3 \times 10^{6}$.

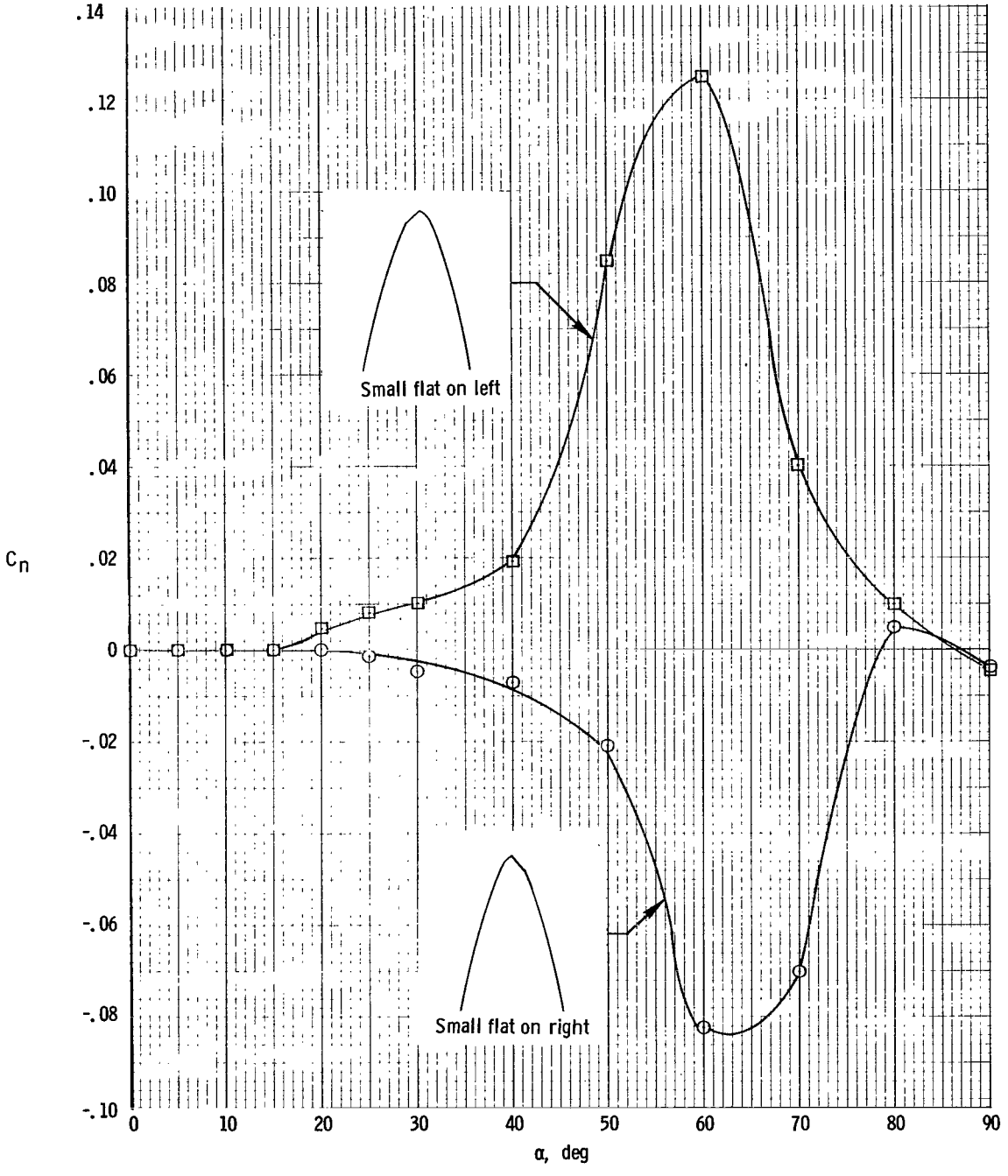

Figure 13.- Effect of dimensional symmetry of nose tip on variation of yawing-moment coefficient with angle of attack. $\beta = 0^{\circ}$; $\Lambda = 50^{\circ}$; $\frac{1}{15}$-scale model; $R = 0.3 \times 10^6$.

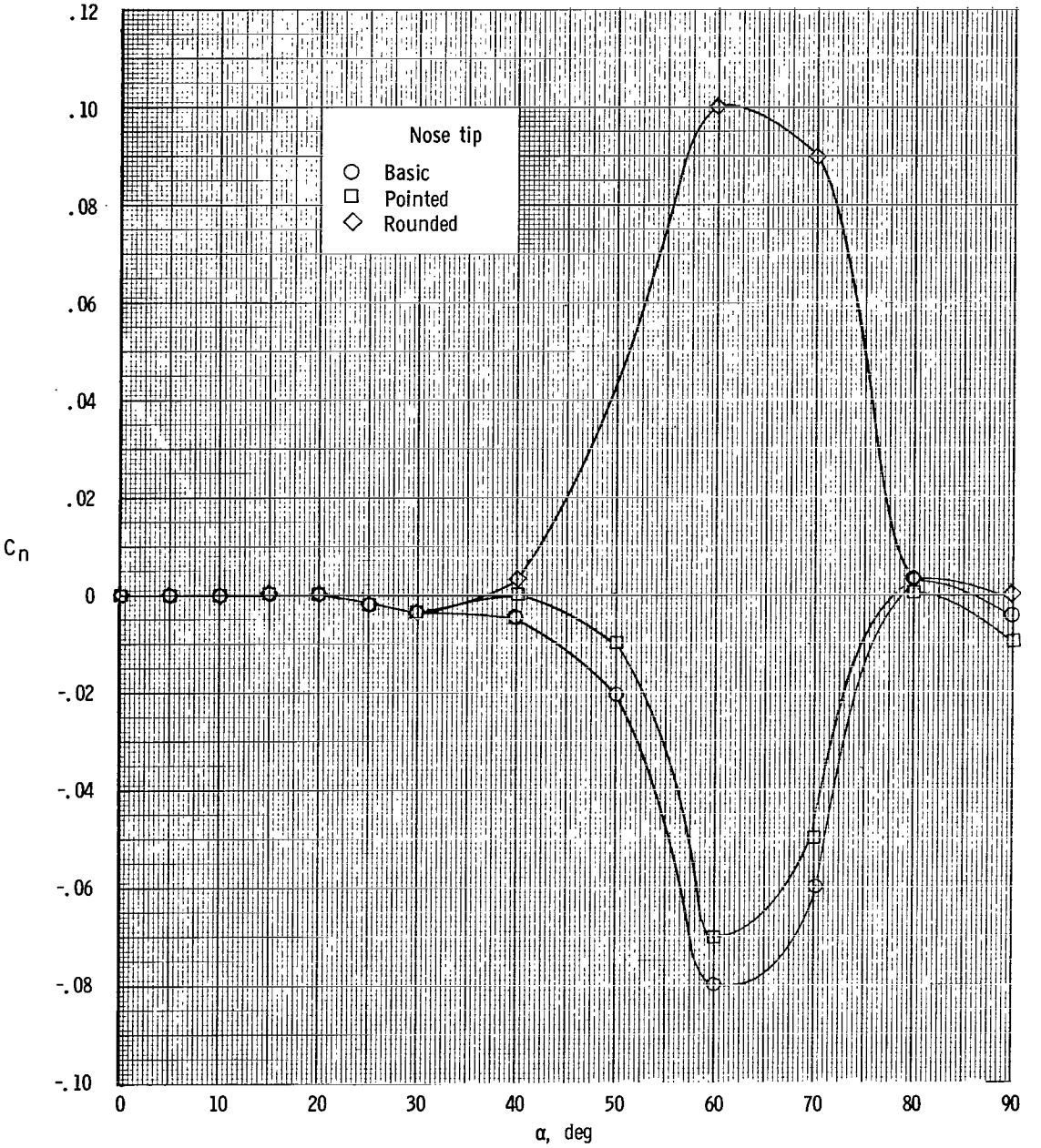

(a) $R = 0.3 \times 10^6$.

Figure 14.- Effect of nose-tip shape on variation of yawing-moment coefficient with angle of attack. $\beta = 0^\circ$; $\Lambda = 50^\circ$; $\frac{1}{15}$-scale model.

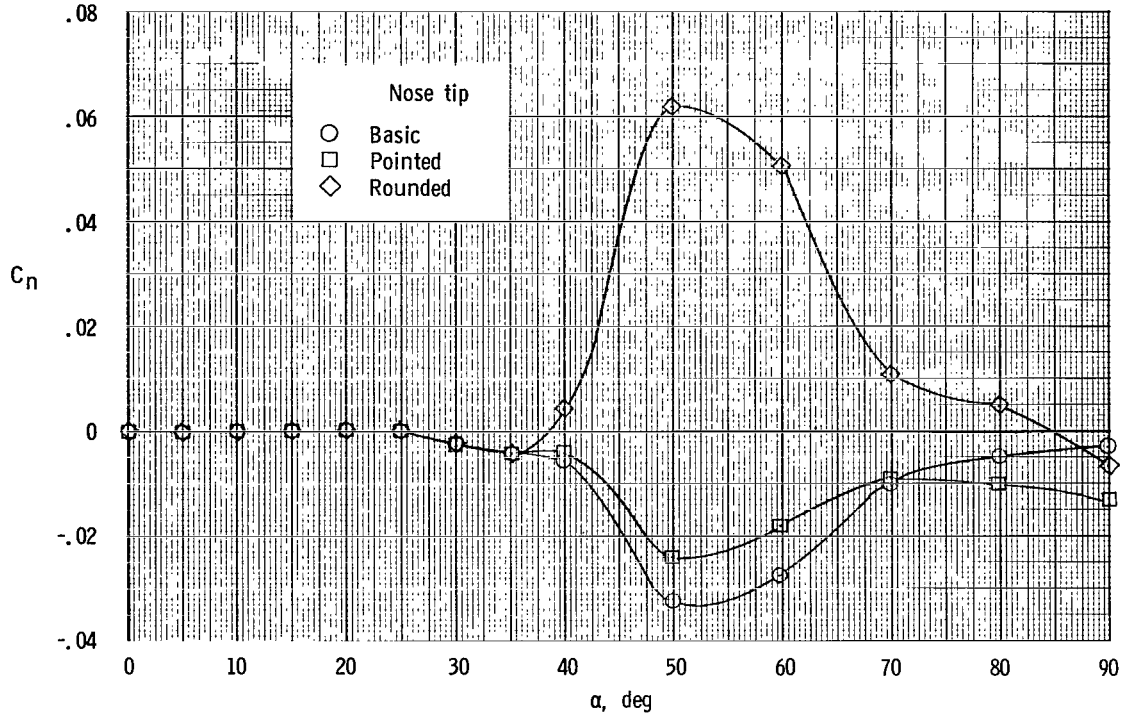

(b) $R = 0.8 \times 10^6$.

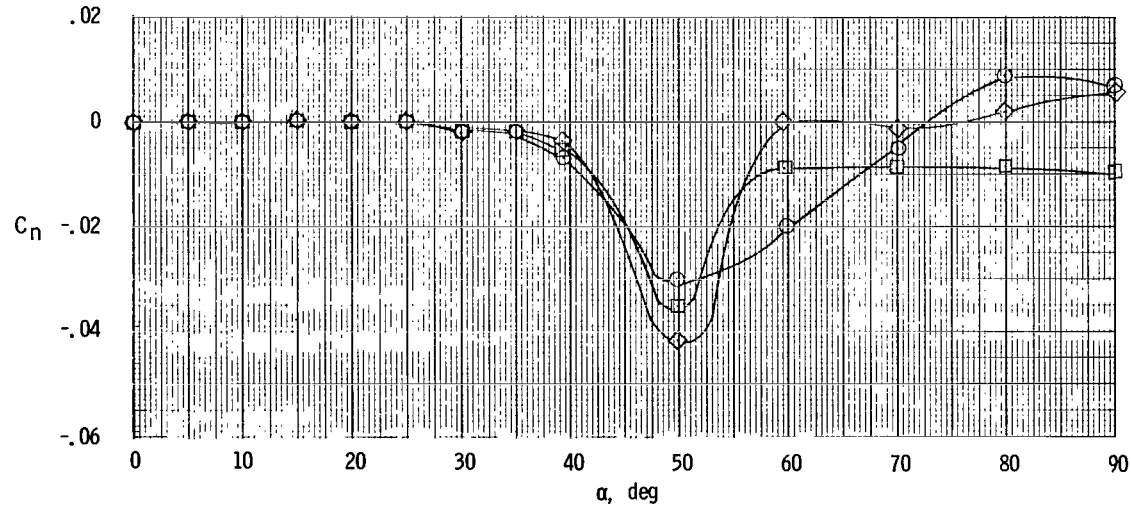

(c) $R = 1.2 \times 10^6$.

Figure 14.- Concluded.

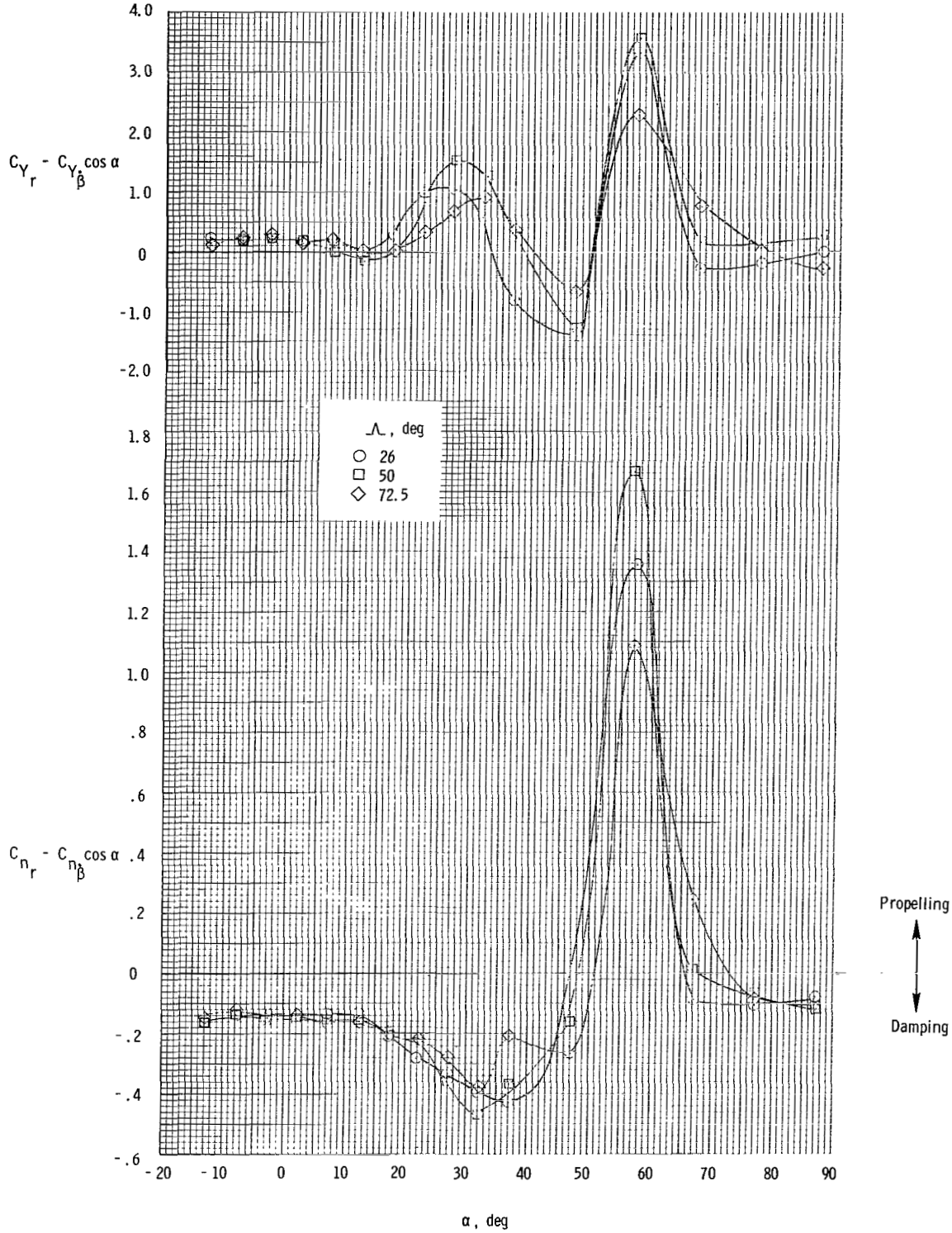

Figure 15.- Variation of aerodynamic damping-in-yaw parameter and side-force-due-to-yawing parameter with angle of attack. $\frac{1}{9}$- scale model; $R = 0.7 \times 10^6$.

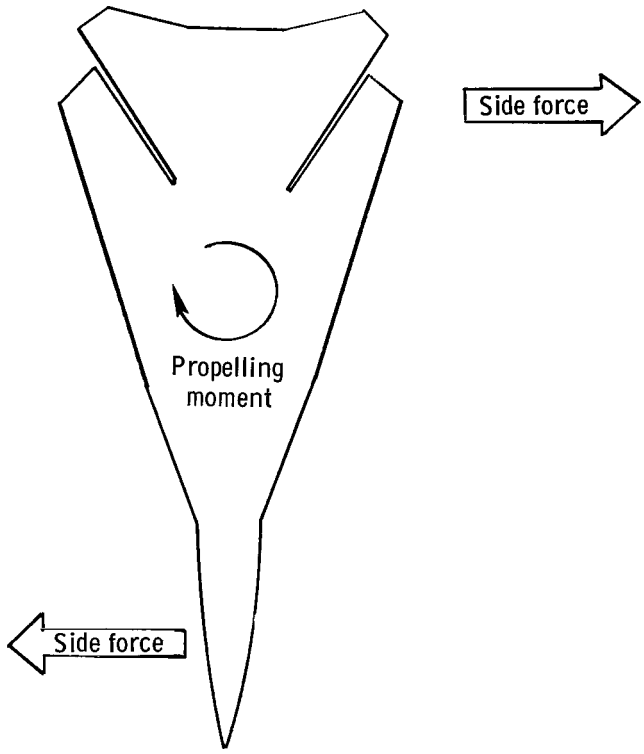

Figure 16.- Assumed relationship between side force and yawing moment during spin to right.

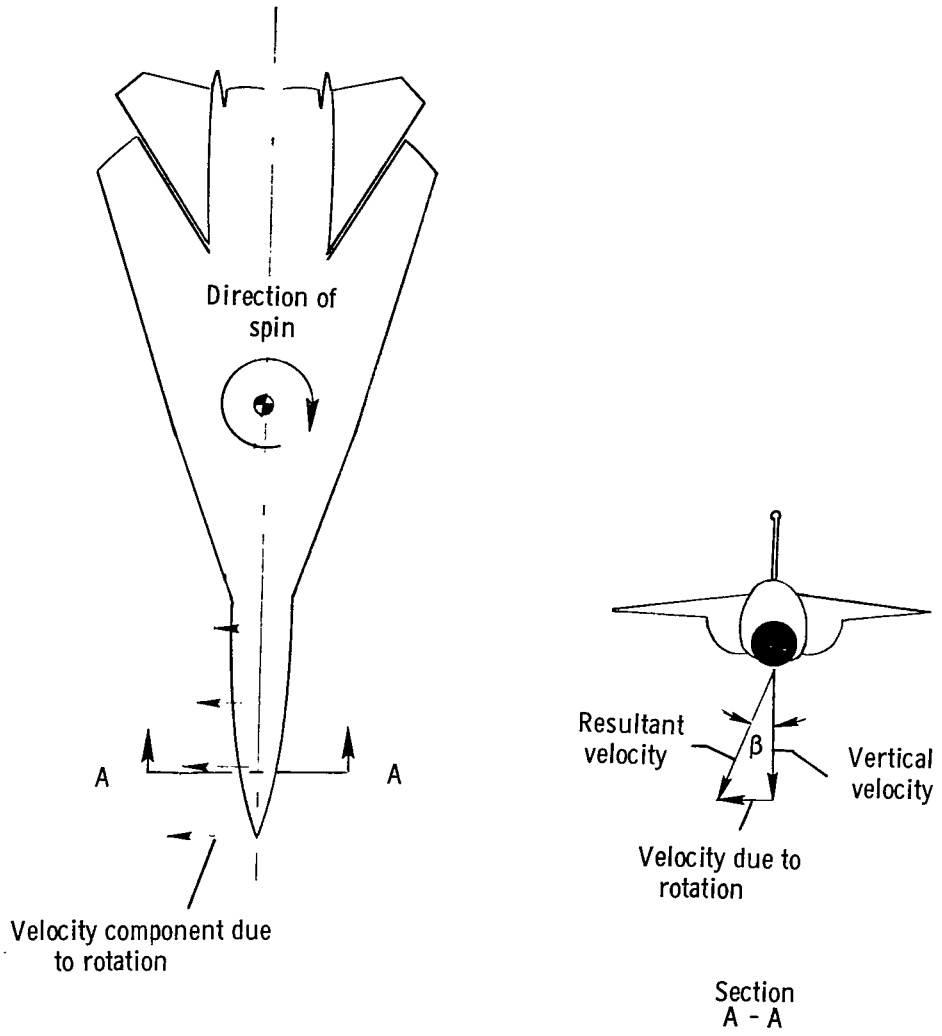

Figure 17.- Sideslip angle generated at nose of airplane during right spin.

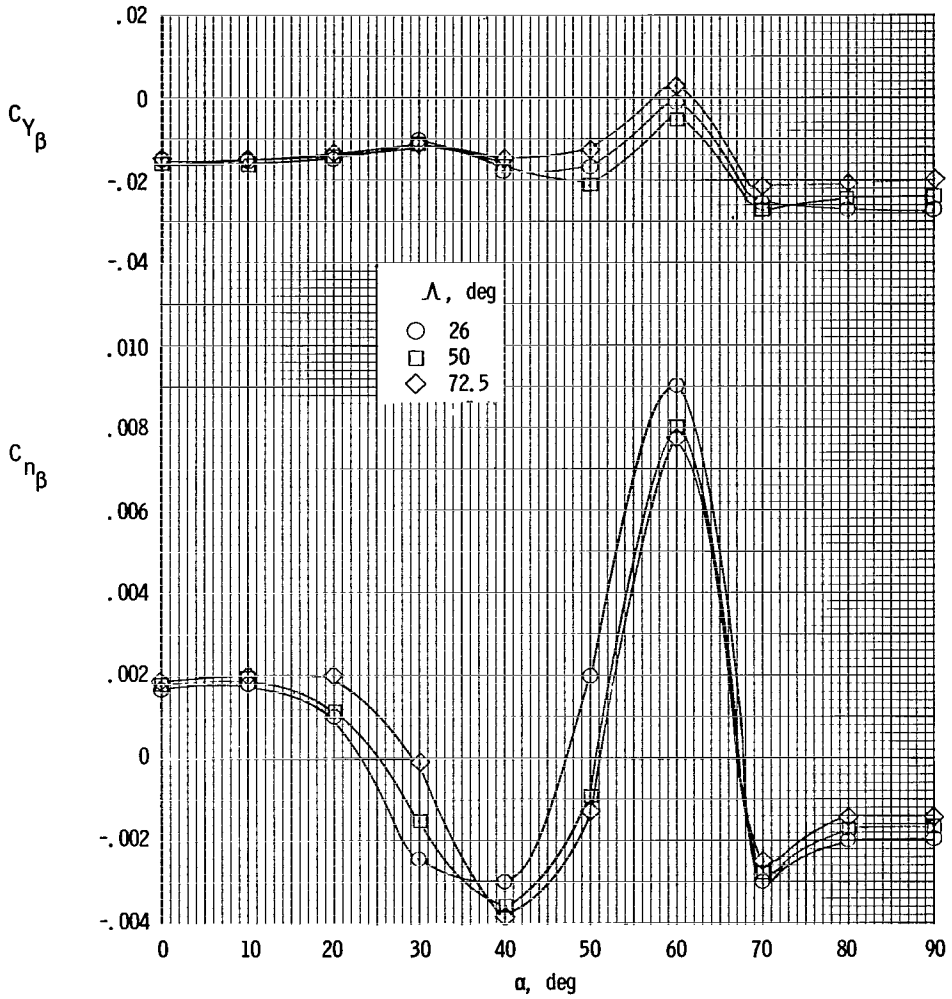

Figure 18.- Effect of wing sweep angle on static stability derivatives C_{Y_β} and C_{n_β}. Data based on measurements at $\beta = \pm 5^\circ$; $\frac{1}{10}$-scale model; $R = 0.3 \times 10^6$.

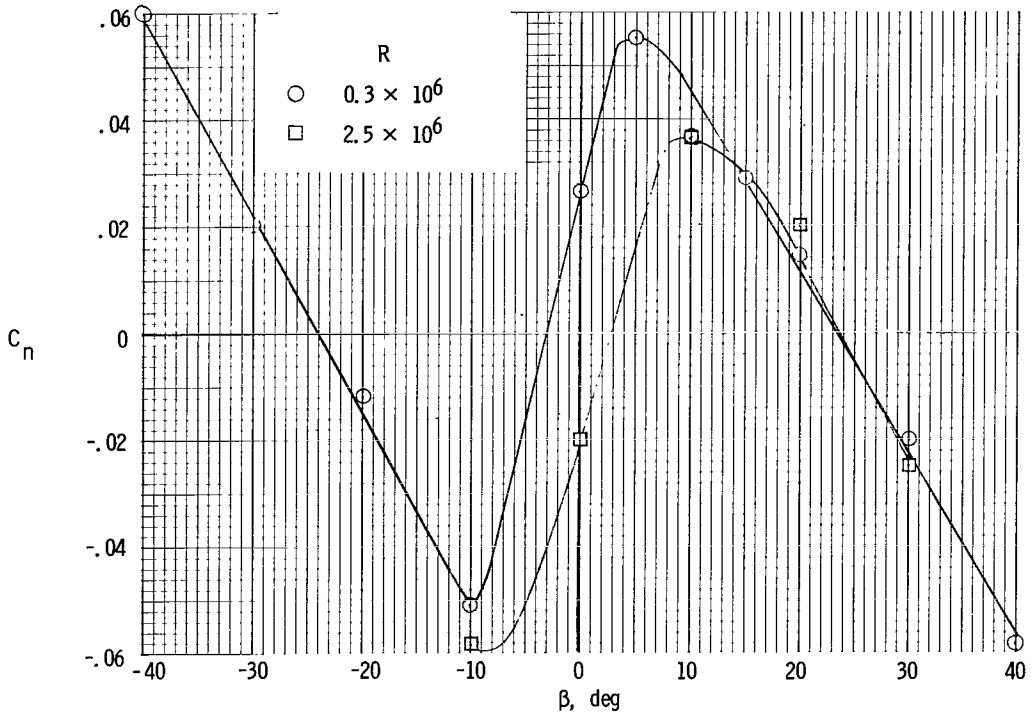

Figure 19.- Variation of yawing-moment coefficient with angle of sideslip. $\alpha = 55^\circ$; $\Lambda = 50^\circ$; $\frac{1}{10}$-scale model.

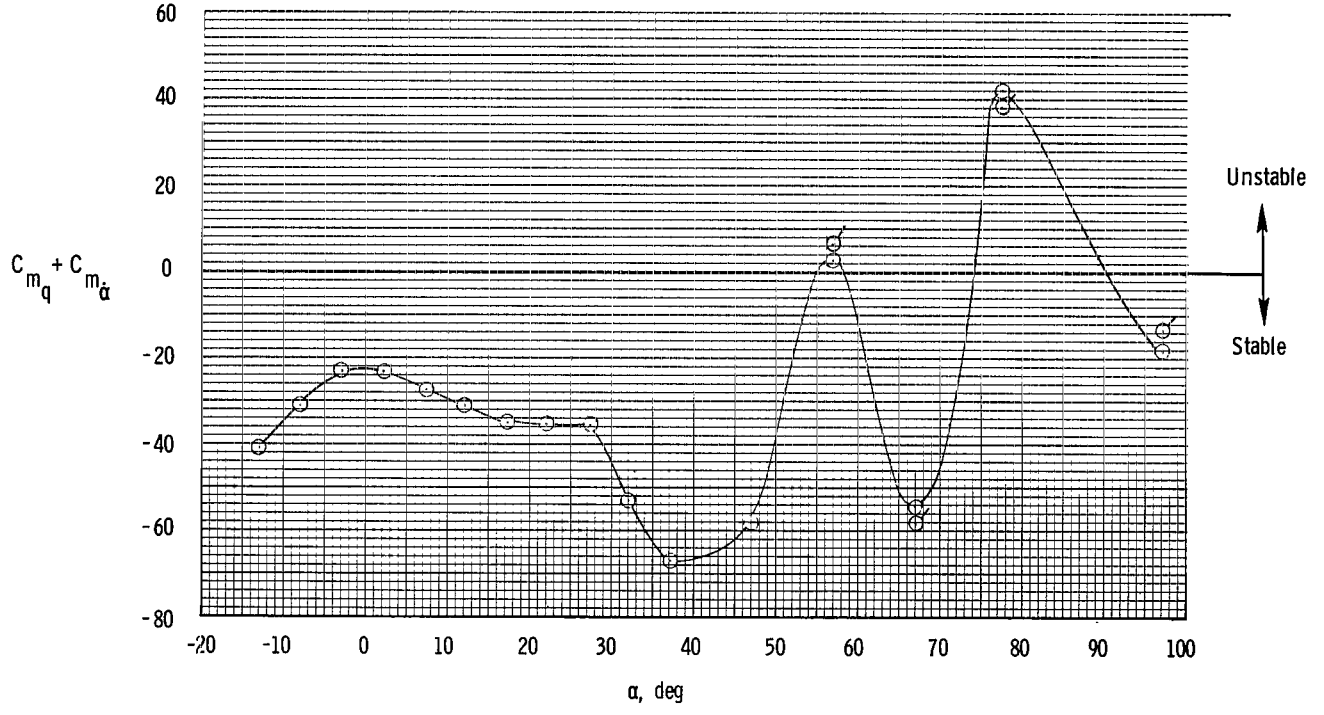

Figure 20.- Variation of aerodynamic damping-in-pitch parameter with angle of attack. $\beta = 0^{\circ}$; $\Lambda = 50^{\circ}$. Flagged symbols indicate repeat tests.

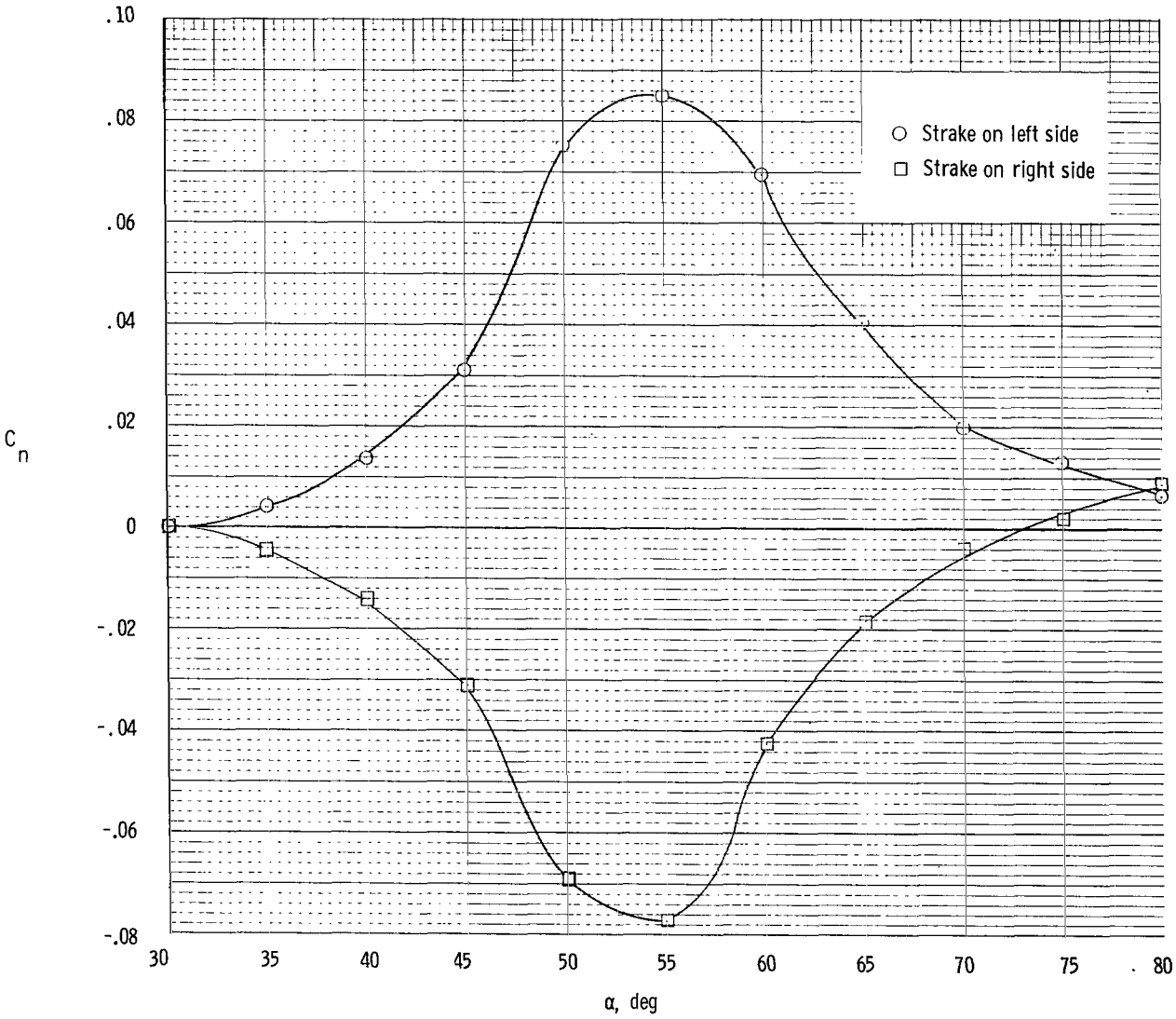

Figure 21.- Effect of single nose strake on variation of yawing-moment coefficient with angle of attack. $\beta = 0^{\circ}$; $\Lambda = 50^{\circ}$; $\frac{1}{10}$-scale model; $R = 0.3 \times 10^{6}$.

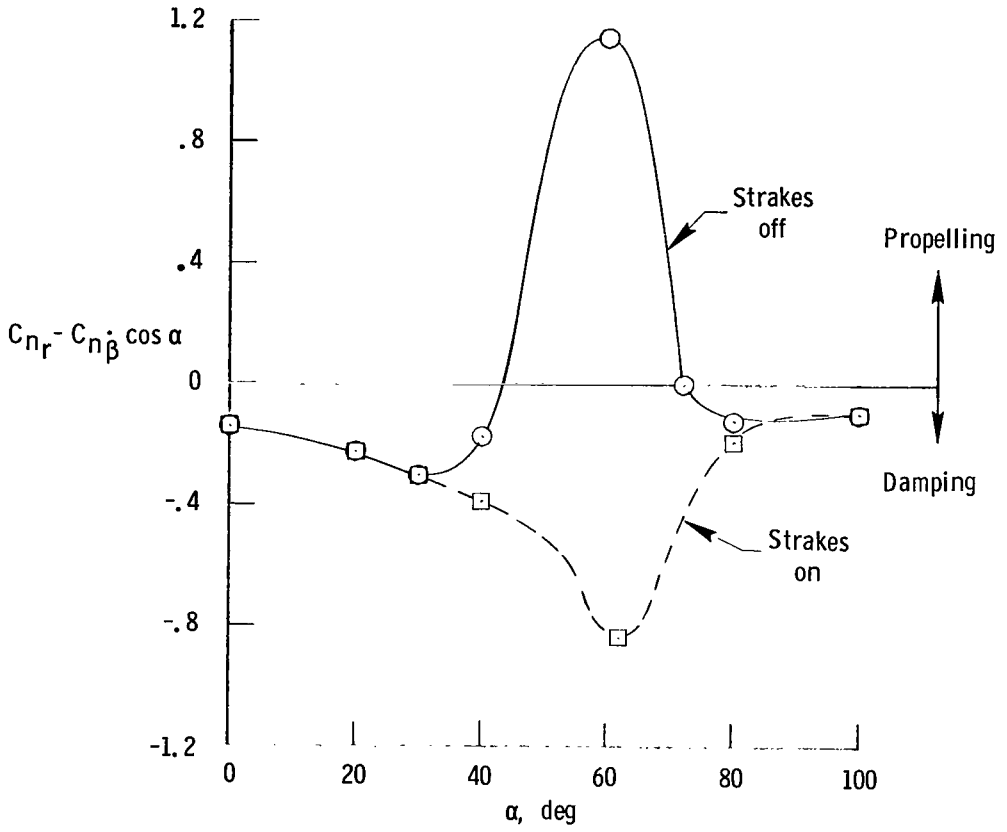

Figure 22.- Effect of double-strake configuration on aerodynamic damping in yaw with angle of attack. $\Lambda = 50^{\circ}$; $\frac{1}{9}$-scale model; $R = 0.7 \times 10^{6}$.

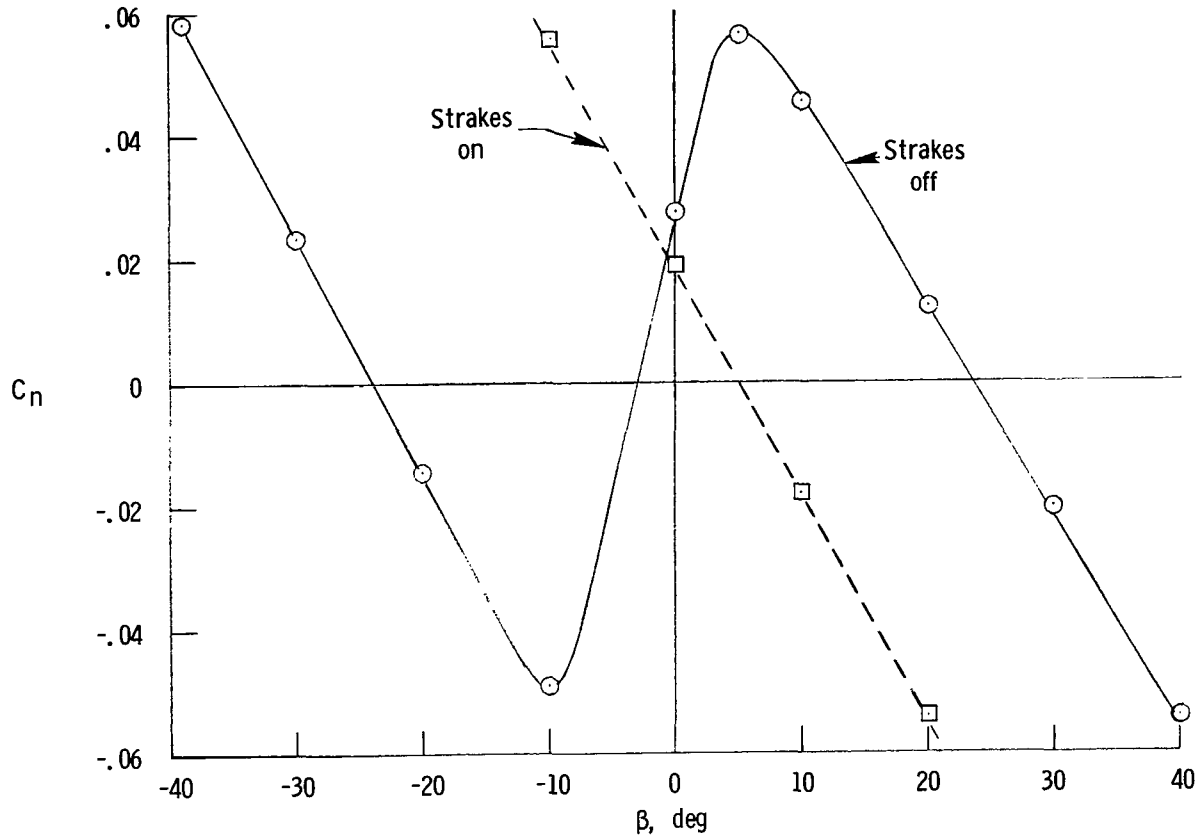

Figure 23.- Effect of double-strake configuration on variation of yawing-moment coefficient with angle of sideslip. $\Lambda = 50^\circ$; $\alpha = 55^\circ$; $\frac{1}{9}$-scale model; $R = 0.7 \times 10^6$.

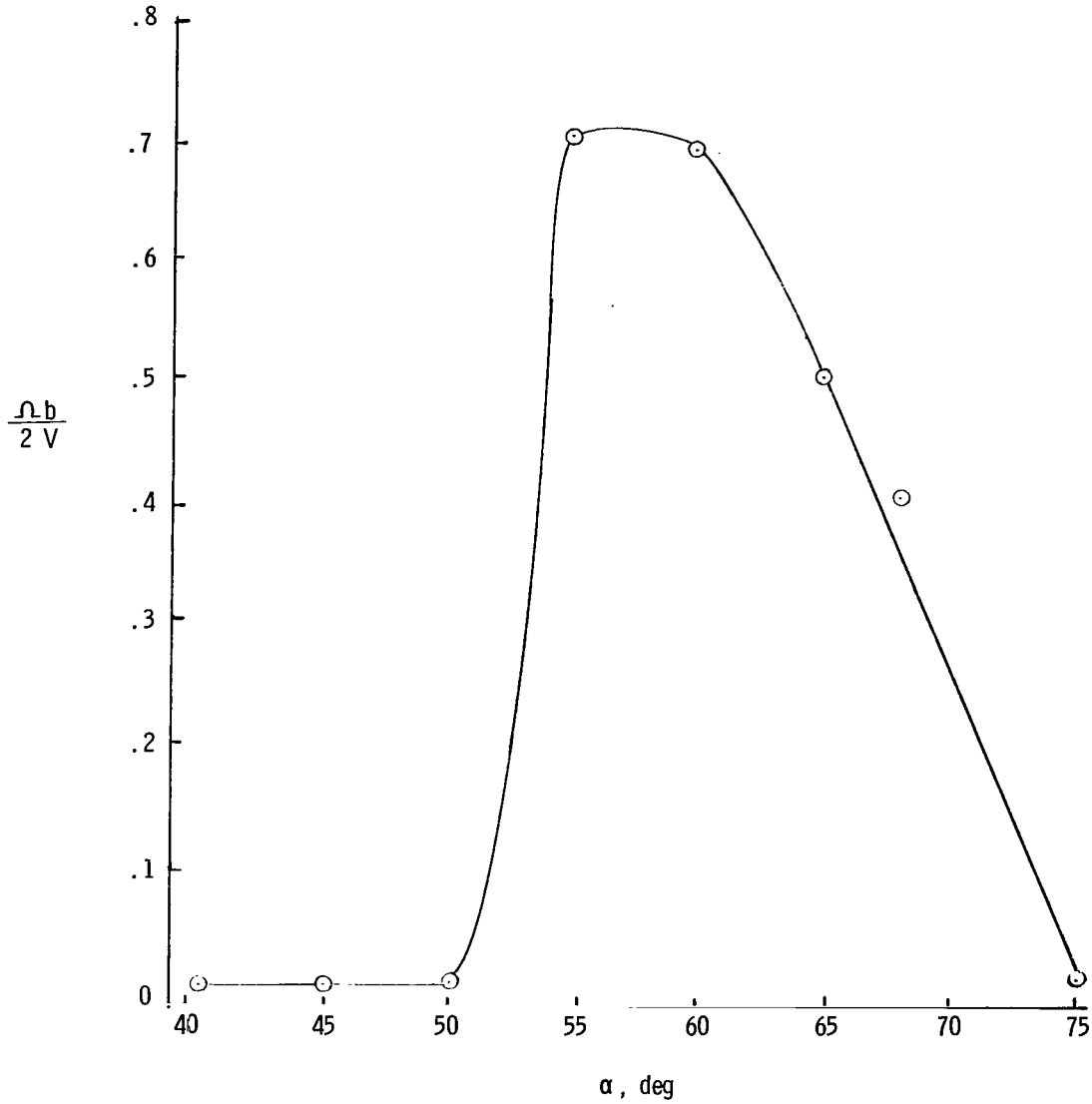

Figure 24.- Variation of nondimensional spin rate with angle of attack as obtained during single-degree-of-freedom autorotation tests. $\Lambda = 50^{\circ}$; $\delta_e = \delta_a = \delta_r = 0^{\circ}$; $\frac{1}{10}$-scale model; $R = 0.3 \times 10^6$.

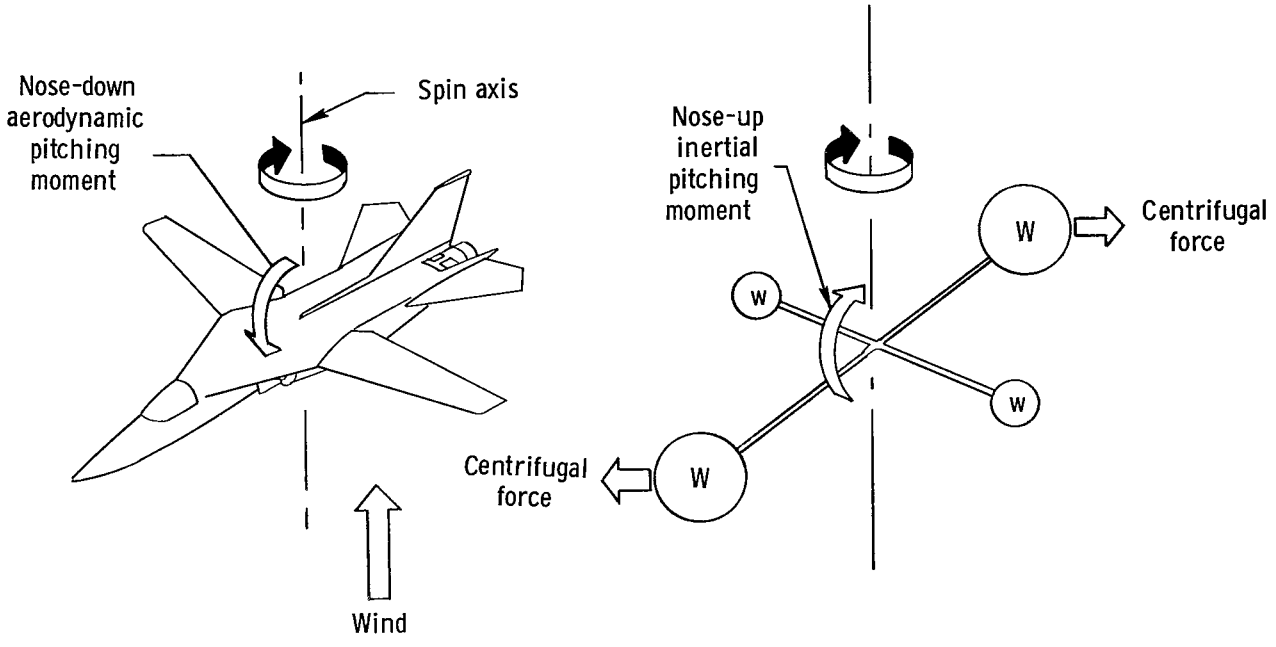

Figure 25.- Balance of aerodynamic and inertial pitching moments during spin.

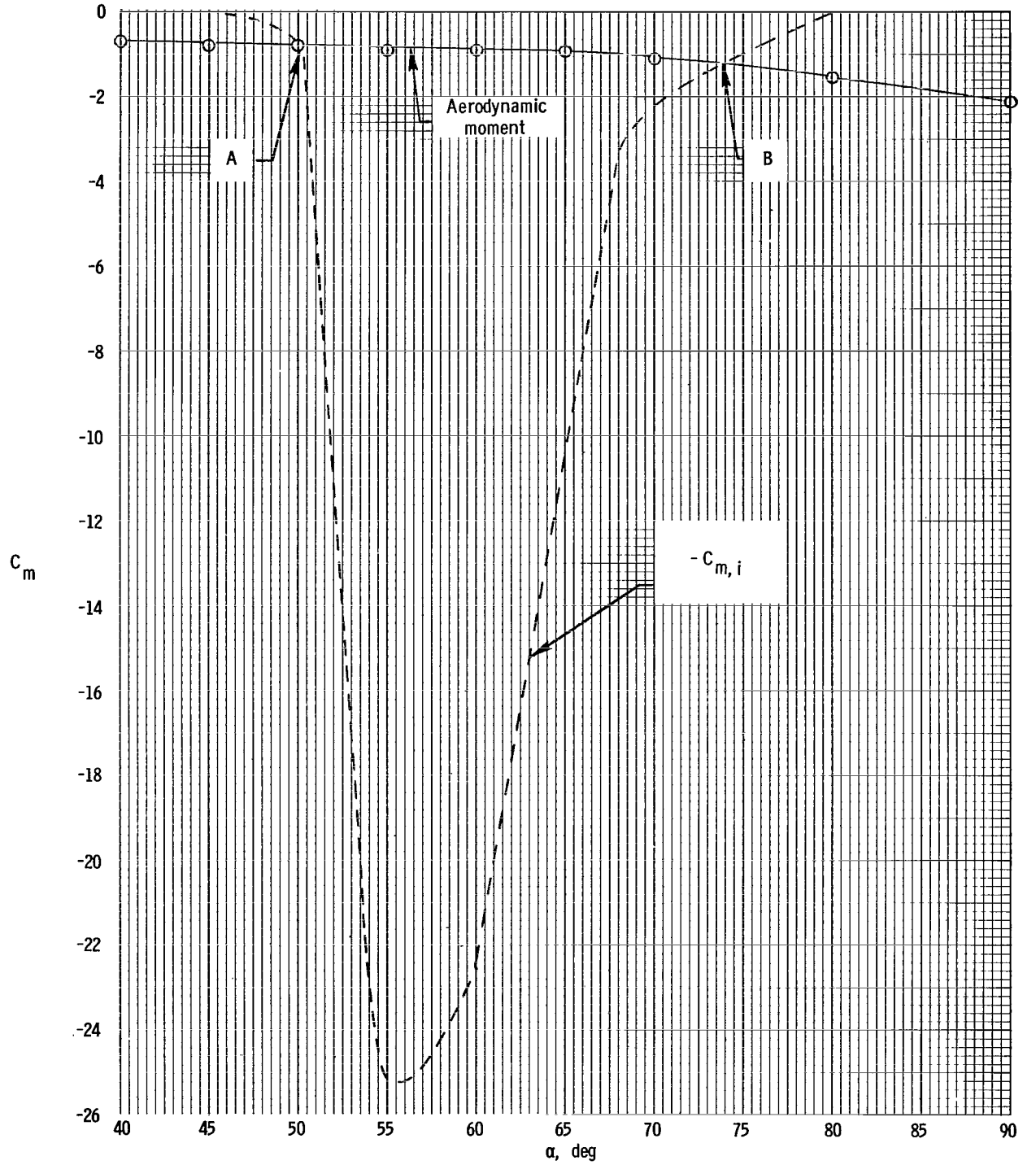

Figure 26.- Variation of aerodynamic and inertial pitching-moment coefficients with angle of attack. Points A and B denote intersection points satisfying balance of inertial and aerodynamic moments. Altitude, sea level; $\Lambda = 50^{\circ}$; $\delta_e = \delta_a = \delta_r = 0^{\circ}$.

NATIONAL AERONAUTICS AND SPACE ADMINISTRATION
WASHINGTON, D. C. 20546
OFFICIAL BUSINESS

FIRST CLASS MAIL

POSTAGE AND FEES PAID
NATIONAL AERONAUTICS AND
SPACE ADMINISTRATION

02U 001 26 51 3DS 70240 00903
AIR FORCE WEAPONS LABORATORY /WLOL/
KIRTLAND AFB, NEW MEXICO 87117

ATT E. LOU BOWMAN, CHIEF,TECH. LIBRARY

POSTMASTER: If Undeliverable (Section 158 Postal Manual) Do Not Return

"The aeronautical and space activities of the United States shall be conducted so as to contribute . . . to the expansion of human knowledge of phenomena in the atmosphere and space. The Administration shall provide for the widest practicable and appropriate dissemination of information concerning its activities and the results thereof."

—NATIONAL AERONAUTICS AND SPACE ACT OF 1958

NASA SCIENTIFIC AND TECHNICAL PUBLICATIONS

TECHNICAL REPORTS: Scientific and technical information considered important, complete, and a lasting contribution to existing knowledge.

TECHNICAL NOTES: Information less broad in scope but nevertheless of importance as a contribution to existing knowledge.

TECHNICAL MEMORANDUMS: Information receiving limited distribution because of preliminary data, security classification, or other reasons.

CONTRACTOR REPORTS: Scientific and technical information generated under a NASA contract or grant and considered an important contribution to existing knowledge.

TECHNICAL TRANSLATIONS: Information published in a foreign language considered to merit NASA distribution in English.

SPECIAL PUBLICATIONS: Information derived from or of value to NASA activities. Publications include conference proceedings, monographs, data compilations, handbooks, sourcebooks, and special bibliographies.

TECHNOLOGY UTILIZATION PUBLICATIONS: Information on technology used by NASA that may be of particular interest in commercial and other non-aerospace applications. Publications include Tech Briefs, Technology Utilization Reports and Notes, and Technology Surveys.

Details on the availability of these publications may be obtained from:

SCIENTIFIC AND TECHNICAL INFORMATION DIVISION

NATIONAL AERONAUTICS AND SPACE ADMINISTRATION

Washington, D.C. 20546